Supporting Information for

Dinuclear Helicate or Mononuclear Pincer Lanthanide Complexes from One Ligand: Stereo-Controlled Assembly and Catalysis

Ran Chen,[a, b] Qian-Qian Yan, [a, b] Shao-Jun Hu,[b, c] Xiao-Qing Guo,[b,c] Li-Xuan Cai,[b] Dan-Ni Yan,[b, c] Li-Peng Zhou, [*b] and Qing-Fu Sun[*a, b, c]

a. College of Chemistry, Fuzhou University, Fuzhou 350108, People's Republic of China.

b. State Key Laboratory of Structural Chemistry, Fujian Institute of Research on the Structure of Matter, Chinese Academy of Sciences, Fuzhou 350002, People's Republic of China.

c. University of Chinese Academy of Sciences, Beijing 100049, People's Republic of China.

Table of contents

1. General
2. Experimental procedures
3. NMR analyses
4. ESI-TOF-MS analyses
5. CD analyses
6. HPLC analyses
7. Single crystal X-ray diffraction analyses
8. References

1. General

Unless otherwise stated, all chemicals and solvents were purchased from commercial companies and used without further purification. Deuterated solvents were purchased from Admas, J&K scientific and Sigma-Aldrich. 1D and 2D-NMR were measured on a Bruker Biospin Avance III (400 MHz) spectrometer or JNM-ECZ600R/S1 (600 MHz) spectrometer. ^{1}H-NMR chemical shifts were determined with tetramethylsilane (TMS) or respect to residual signals of the deuterated solvents used. ESI-TOF-MS were recorded on an Impact II UHR-TOF mass spectrometry from Bruker, with tuning mix as the internal standard. Data analysis was conducted with the Bruker Data Analysis software (Version 4.3) and simulations were performed with the Bruker Isotope Pattern software. X-ray crystallography analysis of single crystal was performed on a Bruker D8 VENTURE photon II diffractometer with Iμs 3.0 microfocus X-ray source diffractometer. Data reduction was performed with the APEX-III software. Structures were solved by direct methods and refined by full-matrix least-squares on F2 with anisotropic displacement using the SHELX software package. Solvent molecules were highly disordered and could not be reasonably located. These residual intensities were removed by PLATON/SQUEEZE routine. Crystal data and final refinement details for the structures are reported in Table S1, S3 and S5. CD spectra were recorded on a MOS-450 circular dichroism spectrometer. HPLC analyses were performed on SHIMADZU LC-20A instrument with chiral AD-H column.

2. Experimental procedures

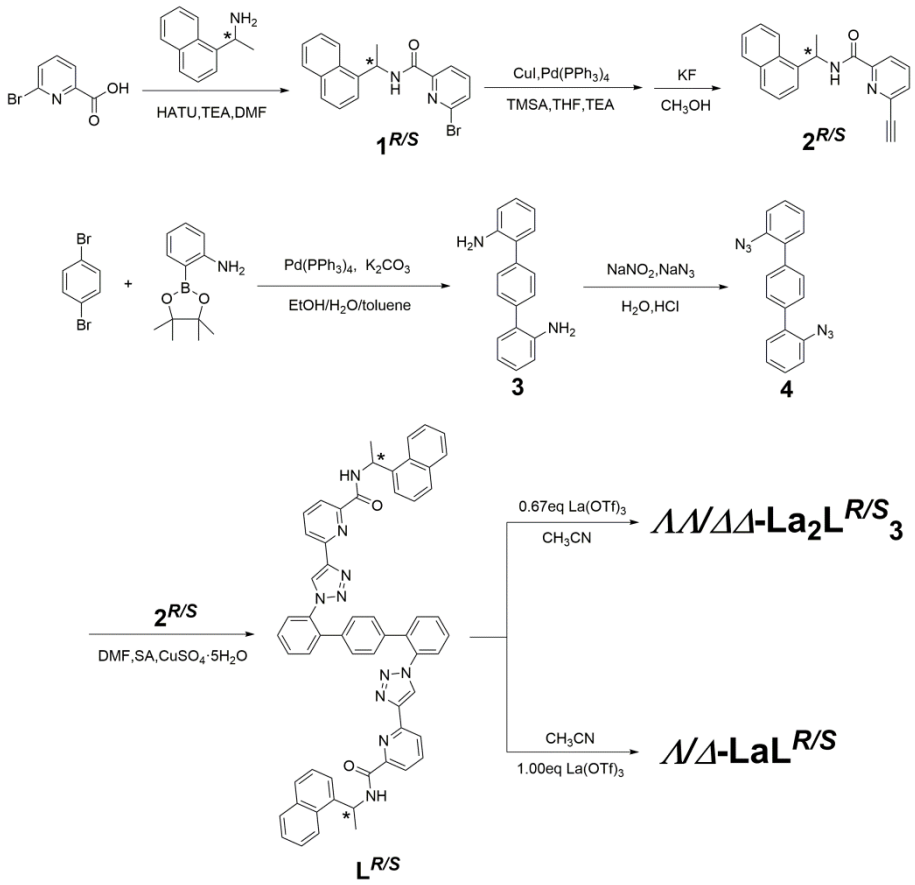

Scheme S1. Synthetic routes of organic ligands $\mathbf{L}^{R/S}$ and the self-assemblies.

Synthesis of compound $\mathbf{1}^{R/S}$: 6-bromopicolinic acid (2.63 g, 13.05 mmol,1.0 equiv), (*R/S*)-1-(naphthalen-1-yl)ethan-1-amine (2.24 g, 13.05 mmol, 1.0 equiv) and DMF (50 mL) were added into a 100 mL one-necked flask. After cooling down to 0 °C with ice water, HATU/2-(7-Aza-1H-Benzotriazole-1-yl)-1,1,3,3-Tetramethyluronium Hexafluorophosphate (7.44 g, 19.58mmol, 1.5equiv) and Et3N (1 mL) were added, then the reaction mixture was stirred for 12 h overnight[1]. The solvent was removed under reduced pressure, and the crude product was purified chromatographically (SiO_2, DCM) to afford $\mathbf{1}^{R/S}$ as pale-yellow grease (4.02 g, 86.8%yield). ^{1}H NMR (600 MHz, $CDCl_3$, 298K) δ 8.20 (d, J = 6.6 Hz, 1H), 8.17 (d, J = 8.6 Hz, 1H), 8.08 (d, J = 8.2 Hz, 1H), 7.88 (d, J = 8.1 Hz, 1H), 7.82 (d, J = 8.2 Hz, 1H), 7.70 (m, 1H), 7.63 (d, J = 7.2 Hz, 1H), 7.59 (d, J = 7.9 Hz, 1H), 7.56 – 7.52 (m, 1H), 7.52 – 7.47 (m, 2H), 6.19 – 6.08 (m, 1H), 1.79 (d, J = 6.8 Hz, 3H). ^{13}C NMR (101 MHz, $CDCl_3$, 298 K) δ = 161.77, 150.97, 140.58, 139.64, 138.14, 133.97, 131.15, 130.79, 128.88, 128.44, 126.59, 125.85, 125.36, 123.33, 122.77, 121.51, 44.91, 21.16. ESI-TOF-MS for $C_{18}H_{15}BrN_2O$ $[M + Na]^+$: calcd, m/z = 377.0260; found, 377.0256.

Synthesis of compound $\mathbf{2}^{R/S}$: $\mathbf{1}^{R/S}$ (4.02g 11.32mmol, 1.0 equiv), CuI (431.20mg, 2.26mmol, 0.2 equiv) and $Pd(PPh_3)_4$ (654.05mg, 0.57mmol, 0.05 equiv) were added into a three-necked flask, and the reaction mixture was stirred in anhydrous Et3N/THF (100 mL, v/v = 1:1) at room temperature under nitrogen atmosphere. Then trimethylsilylacetylene (2.22g, 22.64mmol, 2.0 equiv) was added dropwise into the mixture and the suspension was stirred for 24 h. The residue was filtered off with kieselguhr, and the filtrate was concentrated under reduced pressure. The crude product was then dissolved in MeOH (60 mL) added with KF (626.14mg, 10.78 mmol, 1.3 equiv). The solution was further stirred for 6 h at room temperature. The organic solvent was removed under reduced pressure, and the crude product was purified chromatographically (SiO2, DCM：PE=1:1) to afford $\mathbf{2}^{R/S}$ as yellow grease (2.38 g, 70.1%). ^{1}H NMR (600 MHz, $CDCl_3$, 298K) δ8.23 (m, 2H), 8.18 (d, J = 8.5 Hz, 1H), 7.87 (d, J = 8.1 Hz, 1H), 7.82 (m, 2H), 7.63 (d, J = 7.0 Hz, 1H), 7.58 (d, J = 7.7 Hz, 1H), 7.53 (t, J = 7.0 Hz, 1H), 7.50 – 7.46 (m, 2H), 6.15 (m, 1H), 3.16 (s, 1H), 1.79 (d, J = 6.8 Hz, 3H). ^{13}C NMR (101 MHz, CDCl3, 298 K) δ = 162.39, 150.25, 140.75, 138.23, 137.65, 133.96, 131.19, 129.97, 128.71, 128.37, 126.53, 125.79, 125.31, 123.39, 122.76, 122.32, 82.19, 77.87, 44.79, 21.10. ESI-TOF-MS for $C_{11}H_{12}N_2O$ $[M + Na]^+$: calcd, m/z 323.1155; found: 323.1154.

Synthesis of compound 3: 1,4-dibromobenzene(500mg, 2.12mmol, 1.0 equiv), 2-(4,4,5,5-tetramethyl-1,3,2-dioxaborolan-2-yl)aniline(1.16g, 5.29mmol, 2.5equiv), $Pd(PPh_3)_4$ (245mg, 0.21mmol, 0.1 equiv) and K_2CO_3 (1.17g, 8.48mmol, 4.0 equiv) were added into a three-necked flask. After 30ml toluene/EtOH/H_2O (v/v/v = 5:2:1) mixed solvent was added，the reaction mixture was stirred at 100℃ under nitrogen atmosphere for 24h. The solvent was removed under reduced pressure, and the crude product was purified chromatographically (SiO2, DCM：PE=2:1) to afford **3** as pale yellow solid (468mg, 84.8% yield). ^{1}H NMR (400 MHz, $CDCl_3$, 298K) δ 7.54 (s, 2H), 7.18 (m, 2H), 6.88 – 6.77 (m, 2H), 3.80 (s, 2H). ^{13}C NMR (101 MHz, $CDCl_3$, 298K) δ

143.57, 138.36, 130.47, 129.48, 128.60, 127.20, 118.76, 115.71.

Synthesis of compound 4: To a solution of HCl (2 M, 30 mL), **3**(468mg, 1.80 mmol, 1.0 equiv) was added, and solution was cooled down to 0 °C with ice water. Then $NaNO_2$ (745 mg, 10.8mmol, 6.0 equiv) aqueous solution was dropwise added to the solution and keep for 30 min. Then NaN3 (702 mg, 10.8mmol, 6.0 equiv) aqueous solution was dropwise added to the reaction solution very slowly. After stirring for 5 h, the residue was filtered and washed with water to give **4** as yellow solid (520.6mg, 92.6%yield). ^{1}H NMR (400 MHz, $CDCl_3$, 298K) δ 7.53 (s, 2H), 7.45 – 7.38 (m, 2H), 7.31 – 7.27 (m, 1H), 7.23 (t, J = 7.5 Hz, 1H). ^{13}C NMR (101 MHz, $CDCl_3$, 298K) δ137.31, 137.15, 133.26, 131.30, 129.24, 128.82, 125.01, 118.78. ESI-TOF-MS for $C_{18}H_{12}N_6$ $[M+Na]^+$ calcd, m/z 335.1016; found: 335.1011.

Synthesis of $L^{R/S}$: **4**(231.1mg, 0.74mmol, 1.0 equiv)**,** (R)-6-ethynyl-N-(1-(naphthalen-1-yl)ethyl)picolinamide (**2**$^{R/S}$) (555.6mg, 1.51mmol, 2.5 equiv) were added into mixture of sodium ascorbate (206 mg, 1.04 mmol, 1.4 equiv), CuSO4·5H2O (110 mg, 0.45mmol, 0.6 equiv) and the mixture was stirred at 60 °C for 24 h. After filtration, the solvent was removed under reduced pressure and the crude product was purified chromatographically (SiO2, DCM/MeOH = 10:1) to afford L^R as white solid (464.2 mg, 68.7%yield). ^{1}H NMR (400MHz, CD_3CN, 298K) δ 8.49 (d, J = 8.4 Hz, 1H), 8.44 (s, 1H), 8.16 (d, J = 8.1 Hz, 1H), 8.09 (d, J = 7.7 Hz, 1H), 8.00 (d, J = 7.3 Hz, 1H), 7.93 (t, J = 7.7 Hz, 1H), 7.86 (d, J = 8.8 Hz, 1H), 7.74 (d, J = 8.2 Hz, 1H), 7.58 – 7.51 (m, 4H), 7.50 – 7.43 (m, 2H), 7.43 – 7.39 (m, 1H), 7.36 (t, J = 7.7 Hz, 1H), 6.98 (s, 2H), 5.97 (m, 1H), 1.61 (d, J = 6.9 Hz, 3H). ^{13}C NMR (101 MHz, CD_3CN, 298K) δ 163.40, 140.02, 139.25, 137.66, 131.77, 131.05, 129.37, 129.33, 129.04, 128.25, 127.32, 126.85, 126.26, 126.07, 126.05, 123.65, 123.29, 122.73, 121.67, 45.43, 21.38, 1.52, 1.31. ESI-TOF-MS for $C_{58}H_{44}N_{10}O_2$ $[M+Na]^+$ calcd, m/z 935.3541; found: 935.3527.

Synthesis of *ΛΛ/ΔΔ*-$La_2L^{R/S}_3$: 1.00 eq $L^{R/S}$ (5.5 μmol, 5 mg) was treated with 0.67 eq $La(OTf)_3$ in CD_3CN at 50 °C and stirred for 10 minutes, a homogeneous faint yellow solution was obtained. ^{1}H NMR (400MHz, CD_3CN, 298K) δ8.01 (s, 1H), 7.72 (m, 4H), 7.54 (d, J = 7.4 Hz, 2H), 7.44 (m, 3H), 7.30 (m, 2H), 7.25 – 7.16 (m, 2H), 6.90 (m, 2H), 6.26 (d, J = 7.9 Hz, 1H), 4.94 – 4.85 (m, 1H), 0.76 (d, J = 6.9 Hz, 3H). ^{13}C NMR was not measured due to the poor solubility of such complexes. ESI-TOF-MS for $[(La_2L^R_3)(OTf)]^{5+}$, $[(La_2L^R_3)(OTf)_2]^{4+}$, $[(La_2L^R_3)(OTf)_3]^{3+}$ and $[(La_2L^R_3)(OTf)_4]^{2+}$ calcd, m/z: 632.9719, 828.7037, 1154.5890 and 1806.3598; found:632.9714, 828.7034, 1154.5885 and 1806.3594.

Synthesis of *Λ/Δ*-$LaL^{R/S}$: 1.00 eq $L^{R/S}$ (5.5 μmol, 5 mg) was treated with 1.00 eq $La(OTf)_3$ in CD_3CN at 50 °C and stirred for 10 minutes, a homogeneous faint yellow solution was obtained. ^{1}H NMR (400MHz, CD_3CN, 298K) δ8.77 (d, J = 6.3 Hz, 1H), 8.61 (s, 1H), 8.04 – 7.94 (m, 2H), 7.86 (d, J = 9.2 Hz, 1H), 7.76 (m, 4H), 7.71 – 7.63 (m, 4H), 7.56 – 7.50 (m, 2H), 7.38 (m, 2H), 7.10 (d, J = 6.5 Hz, 1H), 6.84 (d, J = 6.5

Hz, 1H), 6.04 – 5.93 (m, 1H), 1.78 (d, J = 6.4 Hz, 3H). ^{13}C NMR was not measured due to the poor solubility of such complexes. ESI-TOF-MS for $[(LaL^{R})(OTf)]^{2+}$, $[(LaL^{R})(OTf)(H_2O)]^{2+}$ and $[(LaL^{R})(OTf)_2]^{+}$ calcd, m/z: 600.1111, 609.1164 and 1349.1747; found: 600.1108, 609.1155 and 1349.1739.

General procedure for the catalytic reactions: To 0.003 mmol catalyst (based on the molar number of metal center), 2 mmol (300 mg) of trans-β-nitrostyrene and 2 mmol (234 mg) of indole were mixed in $CDCl_3$ up to 800 μL. The mixture was stirred at -5°C for 60 h (or 24 h at rt). For kinetic studies, an aliquot solution (20 μL) of the reaction mixture have been taken out from the system every 1 h and subjected to ^{1}H NMR measurements. Yields were determined by addition of 1,3,5-trimethylbenzene (0.33 eq of trans-β-nitrostyrene) as the internal standard.

3. NMR spectra.

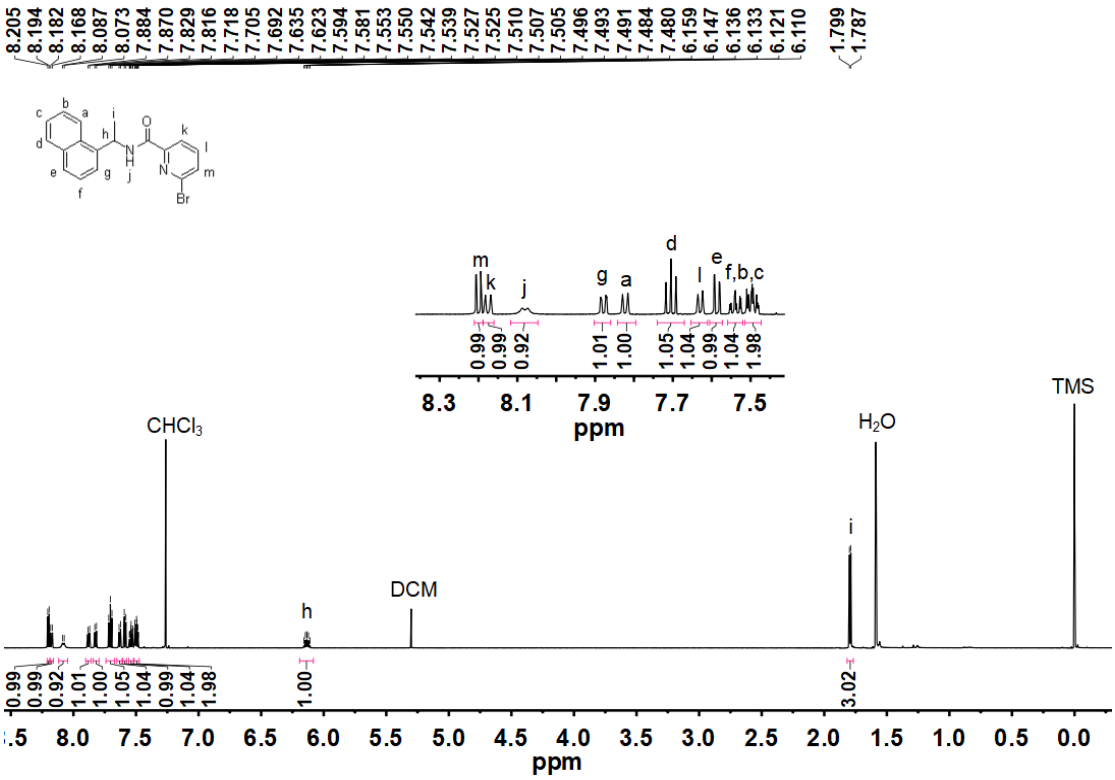

Fig. S1 ^{1}H NMR spectrum of $\mathbf{1}^{R/S}$ (600MHz, $CDCl_3$, 298K).

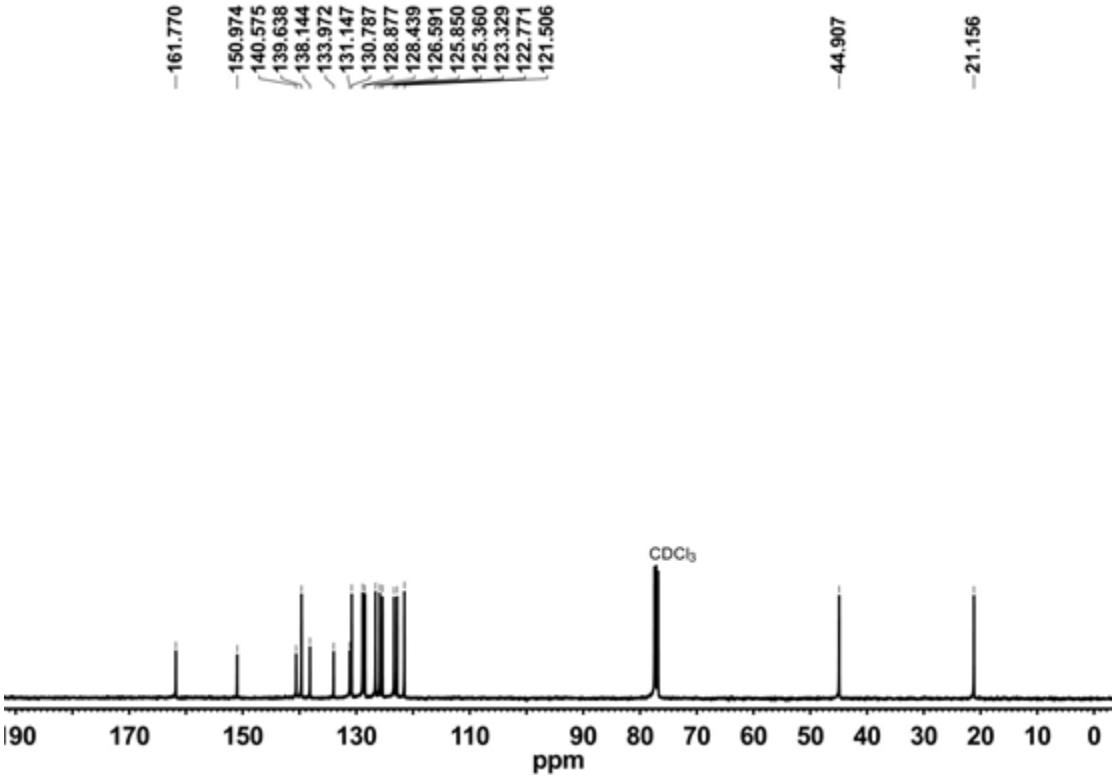

Fig. S2 ^{13}C NMR spectrum of **1**$^{R/S}$ (101MHz, $CDCl_3$, 298K).

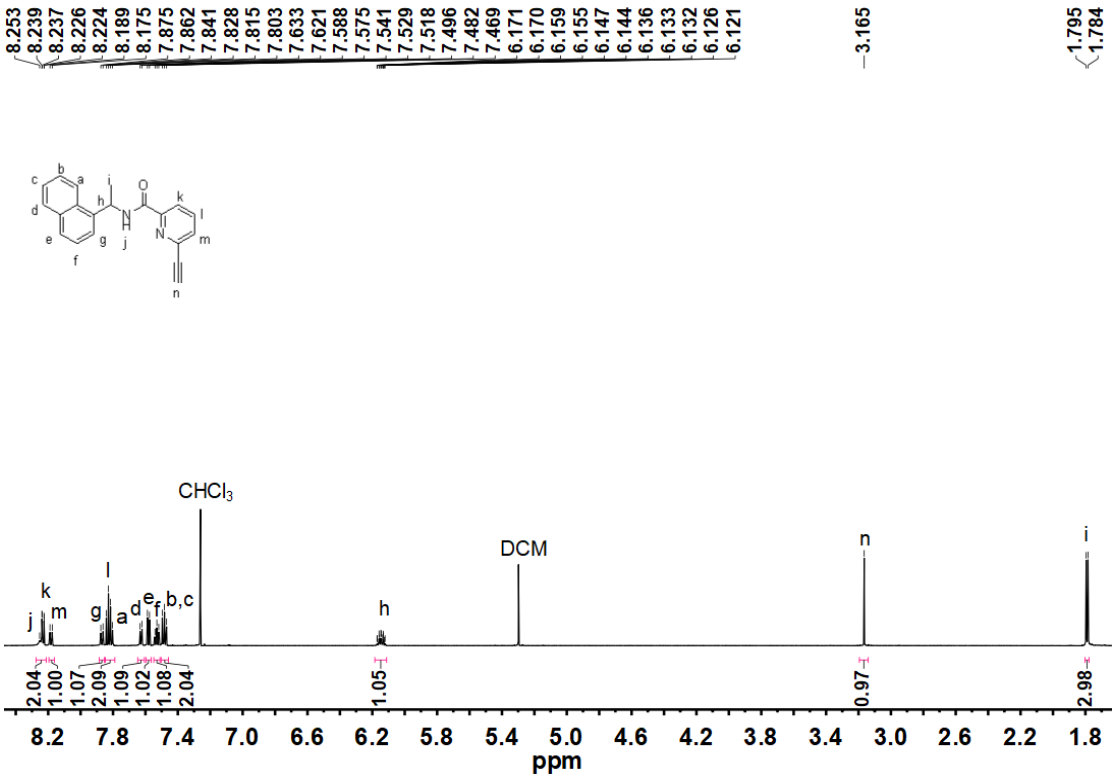

Fig. S3 ^{1}H NMR spectrum of **2**$^{R/S}$ (600MHz, $CDCl_3$, 298K).

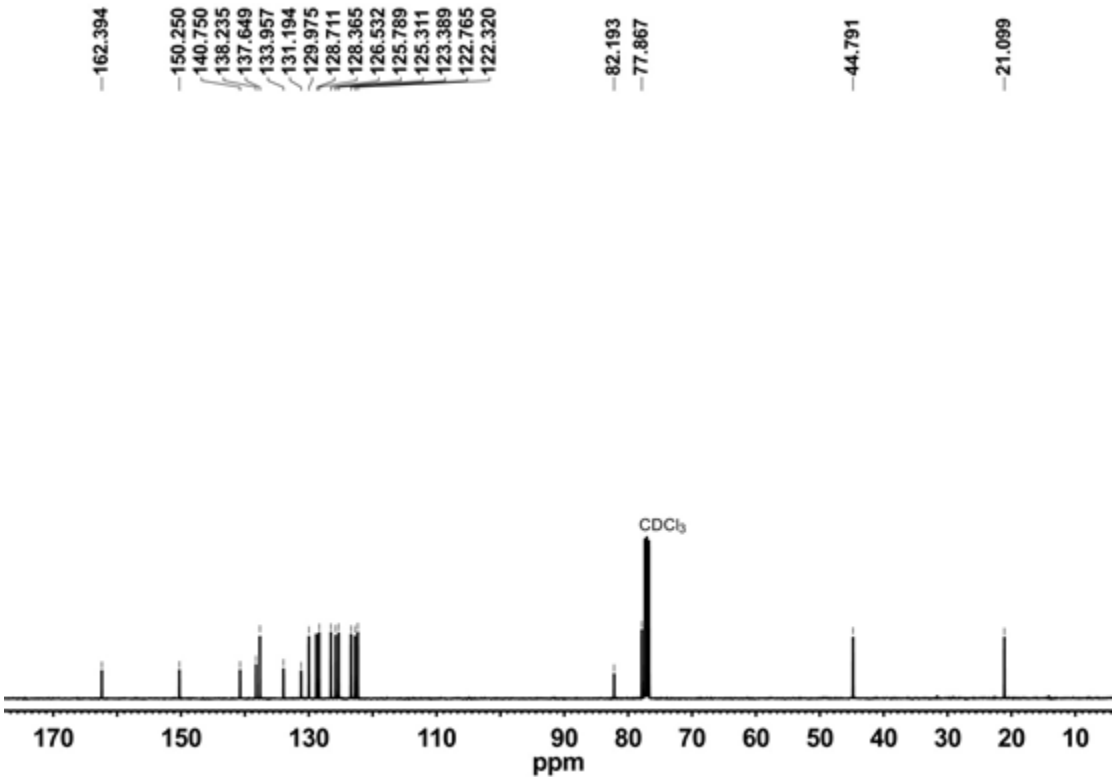

Fig. S4 ^{13}C NMR spectrum of **2**$^{R/S}$ (101MHz, $CDCl_3$, 298K).

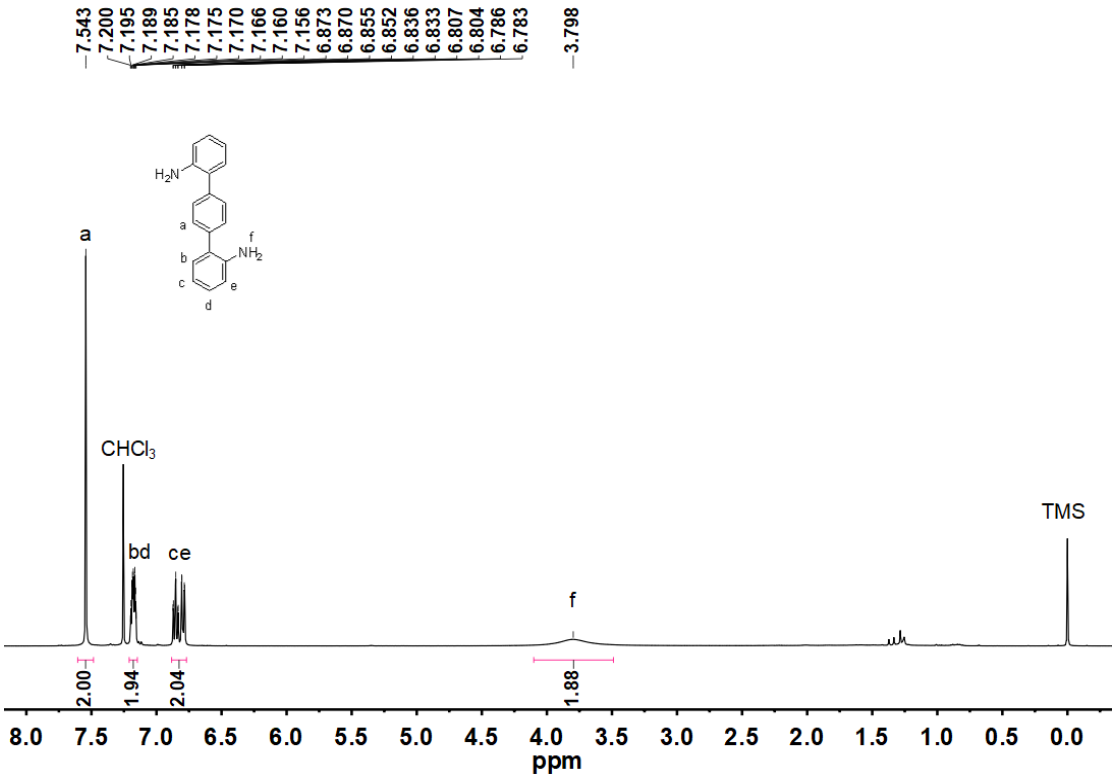

Fig. S5 ^{1}H NMR spectrum of **3** (400MHz, $CDCl_3$, 298K).

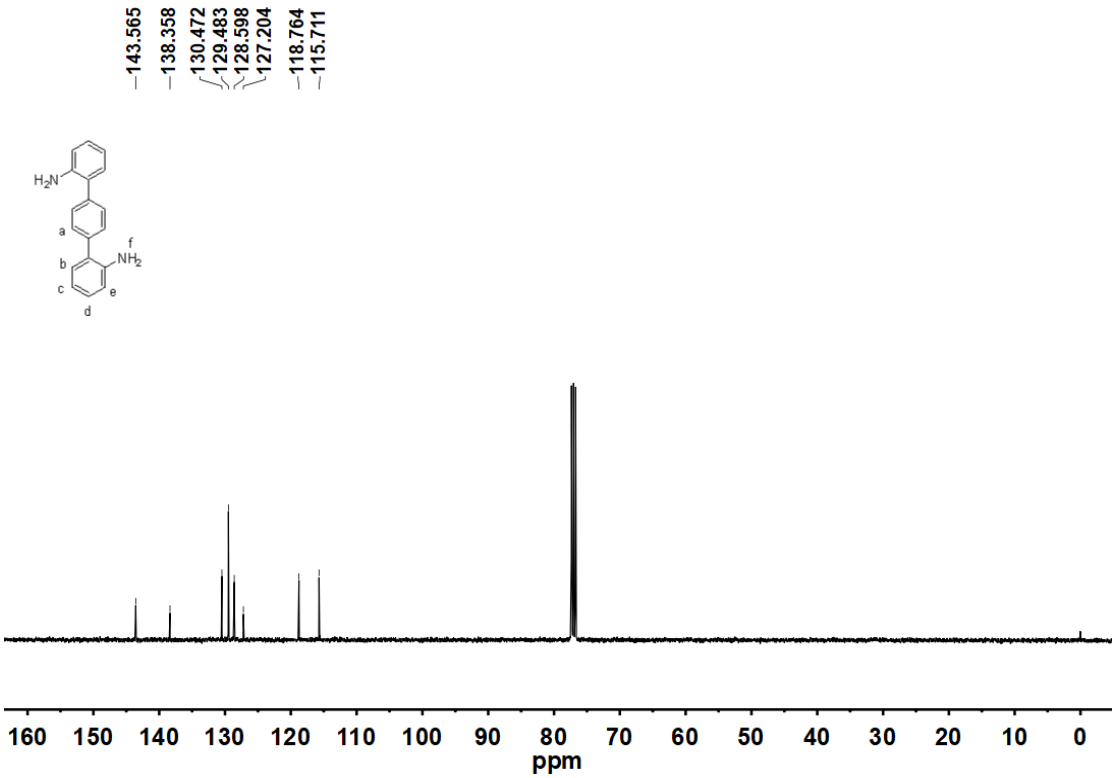

Fig. S6 ^{13}C NMR spectrum of **3** (101MHz, $CDCl_3$, 298K).

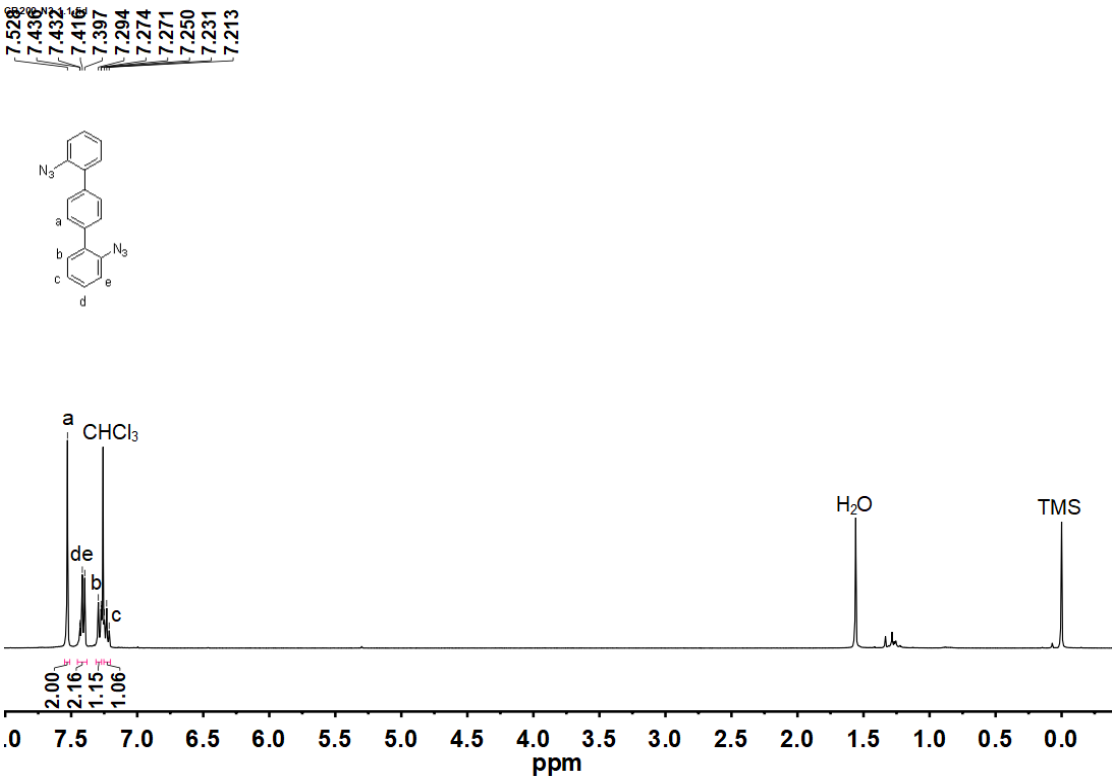

Fig. S7 ^{1}H NMR spectrum of **4** (400MHz, $CDCl_3$, 298K).

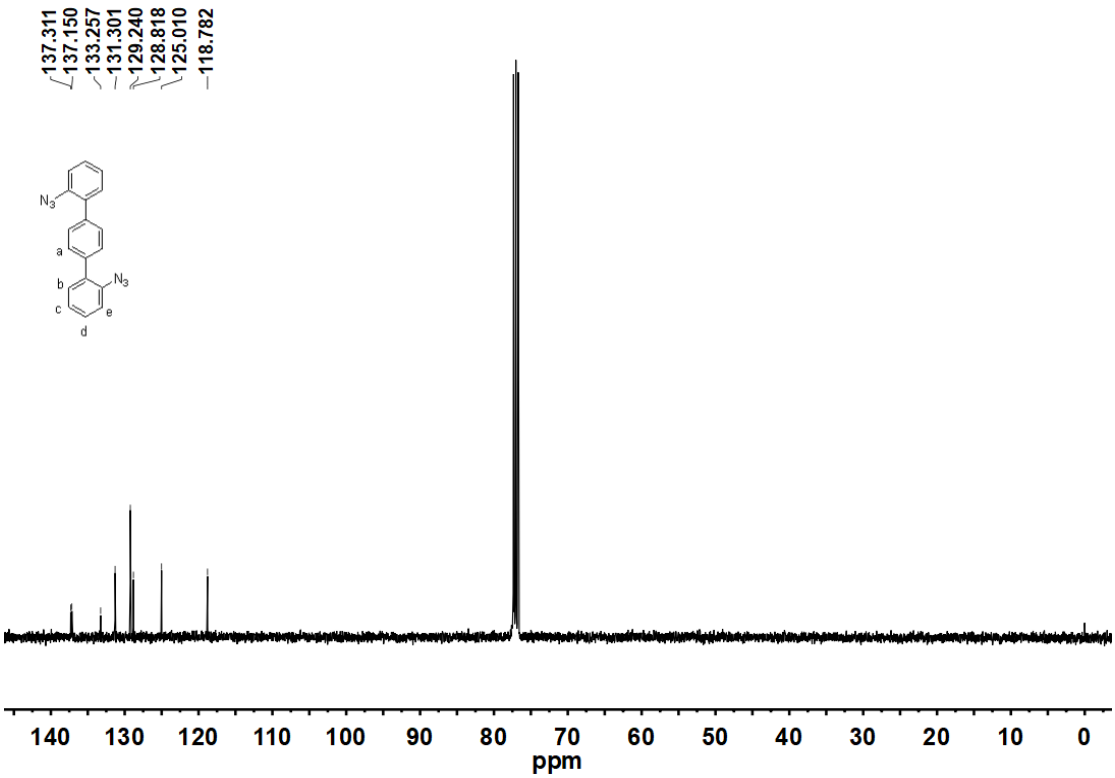

Fig. S8 ^{13}C NMR spectrum of **4** (101MHz, $CDCl_3$, 298K).

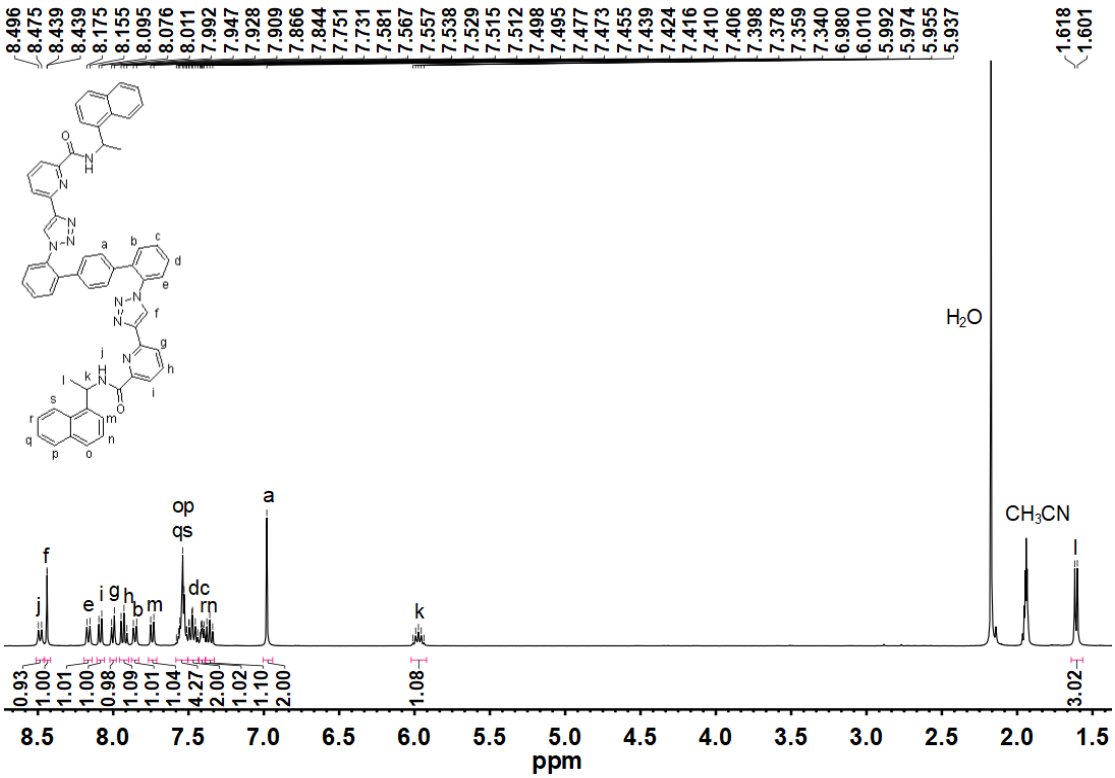

Fig. S9 ^{1}H NMR spectrum of $\mathbf{L}^{R/S}$ (400MHz, CD_3CN, 298K).

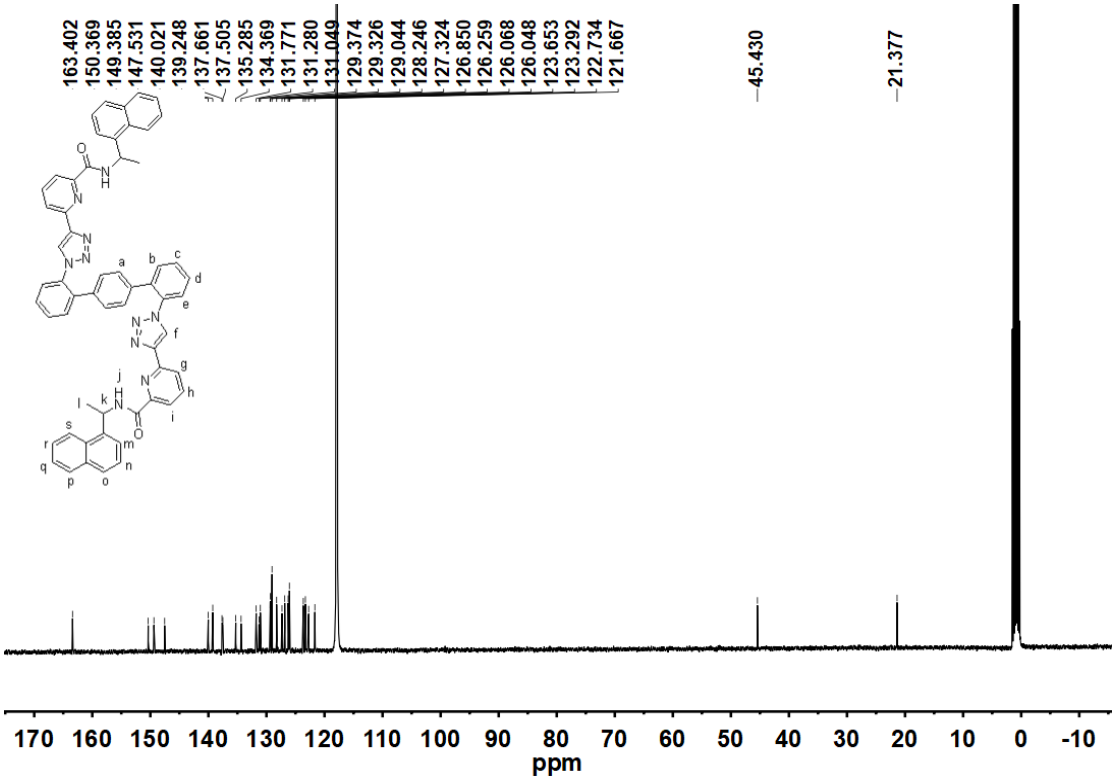

Fig. S10 ^{13}C NMR spectrum of $\mathbf{L}^{R/S}$ (101MHz, CD_3CN, 298K).

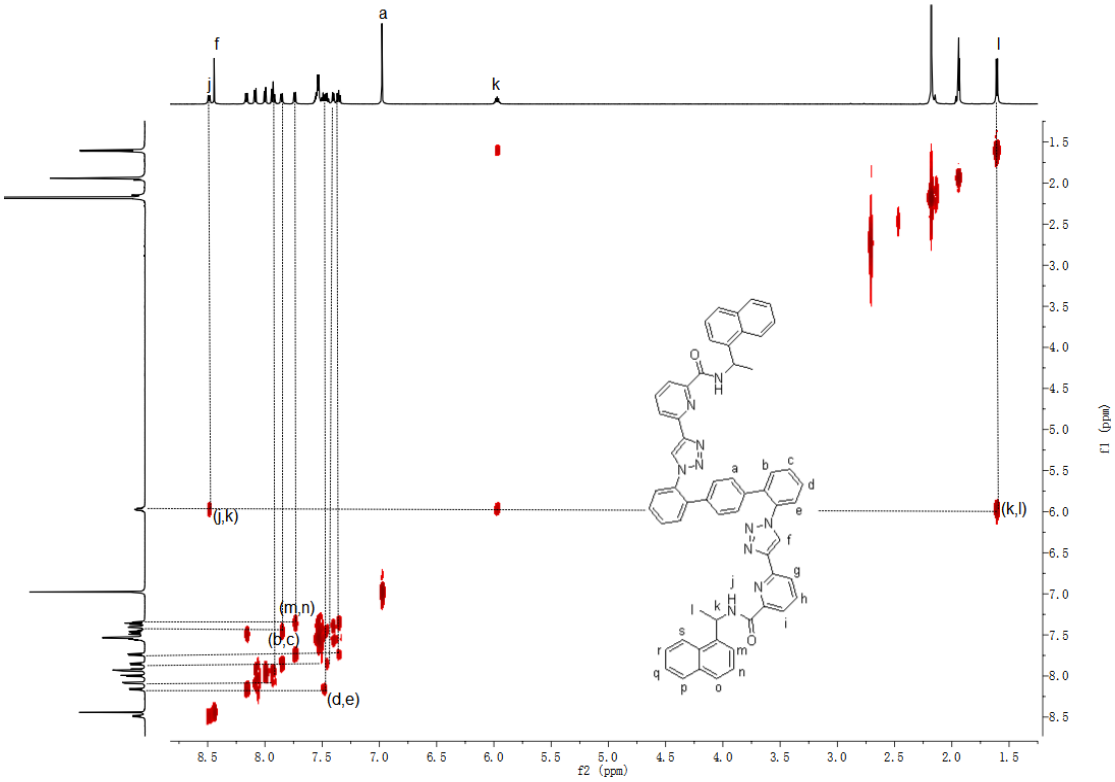

Fig. S11 ^{1}H-^{1}H COSY NMR spectrum of $\mathbf{L}^{R/S}$ (400 MHz, CD_3CN, 298 K).

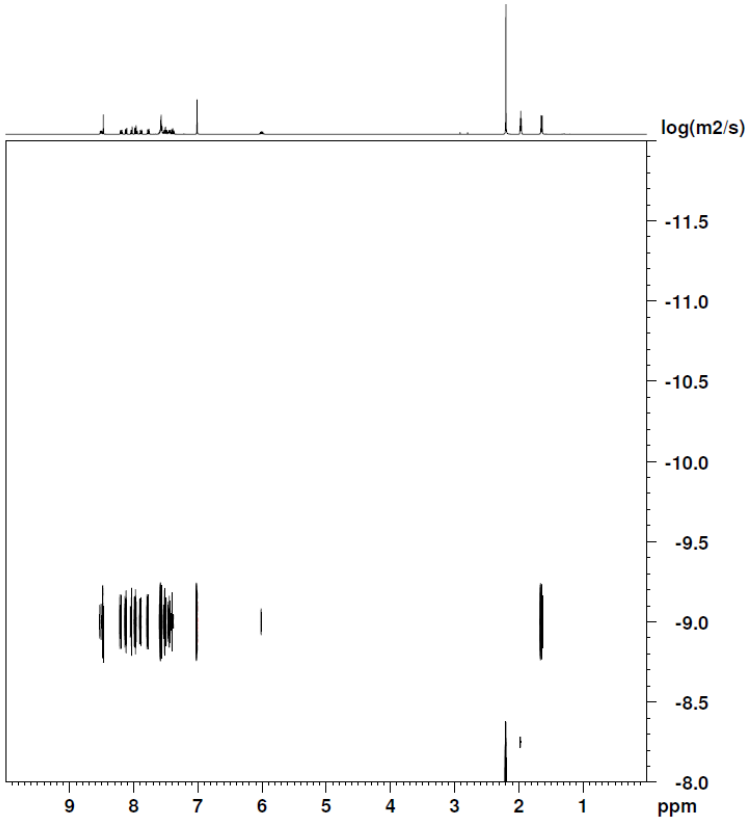

Fig. S12 ^{1}H DOSY spectrum of $\mathbf{L}^{R/S}$ (D = 9.772×10^{-10} m^{2}s^{-1}, r = 6.51Å, 400 MHz, CD_3CN, 298 K).

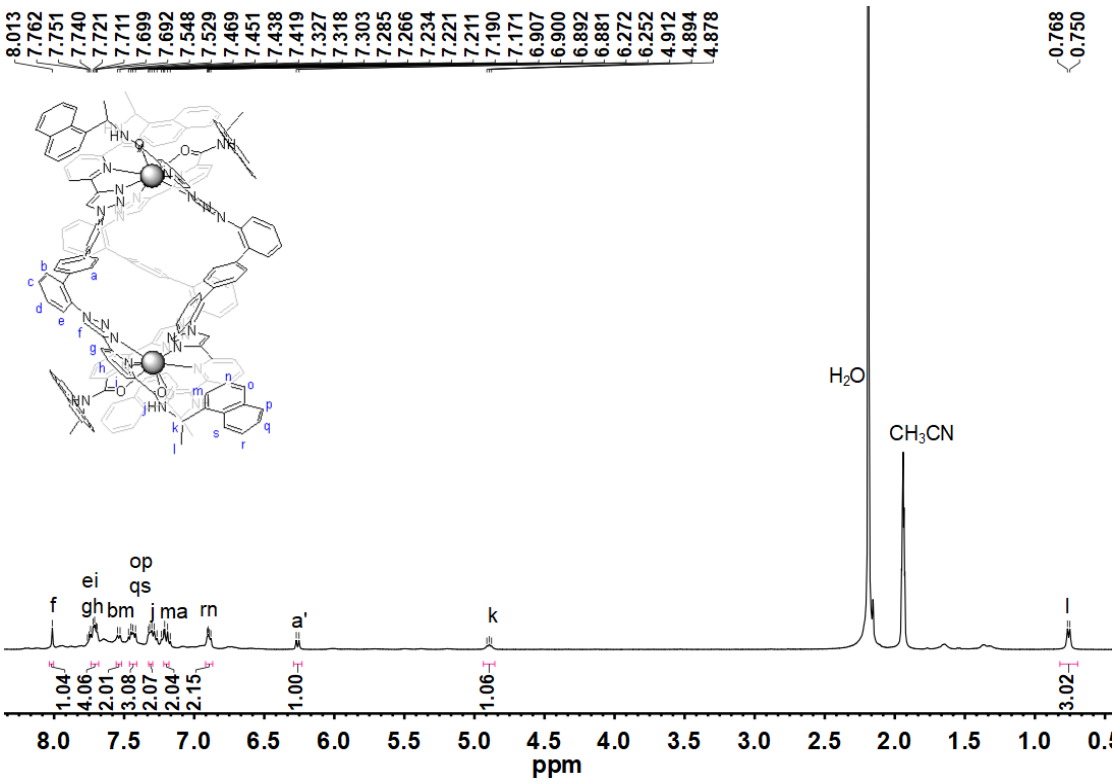

Fig. S13 ^{1}H NMR spectrum of $\Lambda\Lambda/\Delta\Delta$-$\mathbf{La_2L}^{R/S}_3$ (400MHz, CD_3CN, 298K).

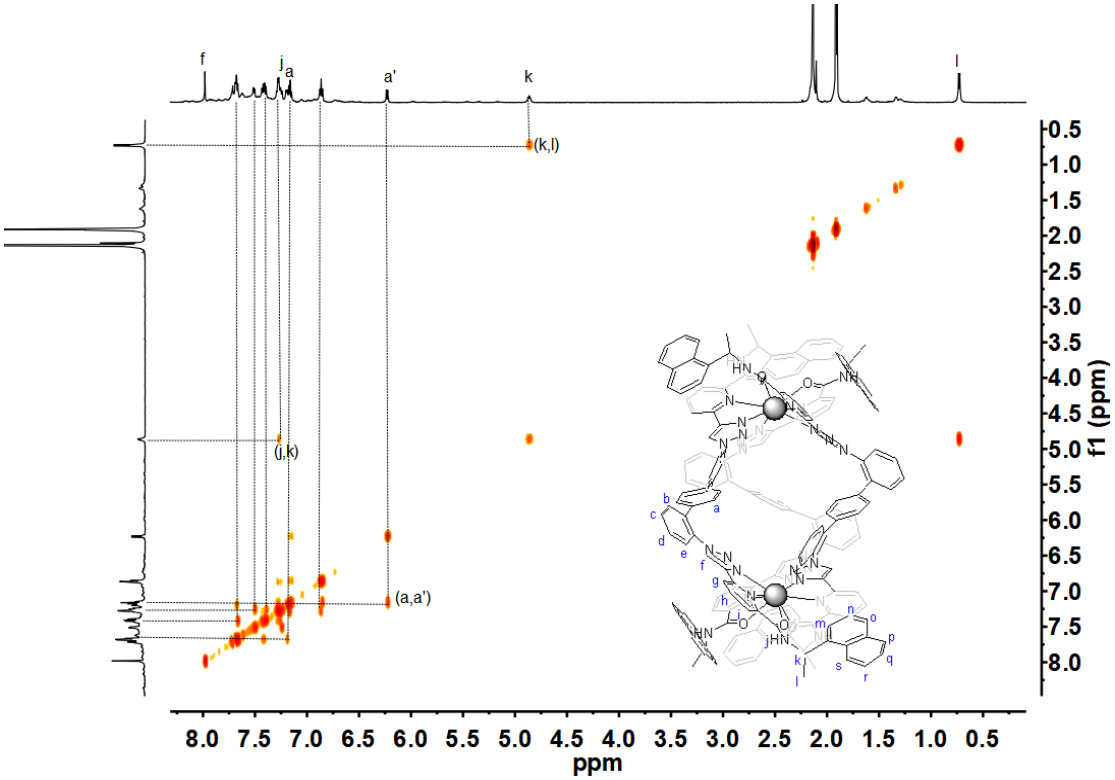

Fig. S14 ^{1}H-^{1}H COSY NMR spectrum of ***ΛΛ/ΔΔ*-La$_2$L$^{R/S}_3$** (400 MHz, $CDCl_3$, 298 K).

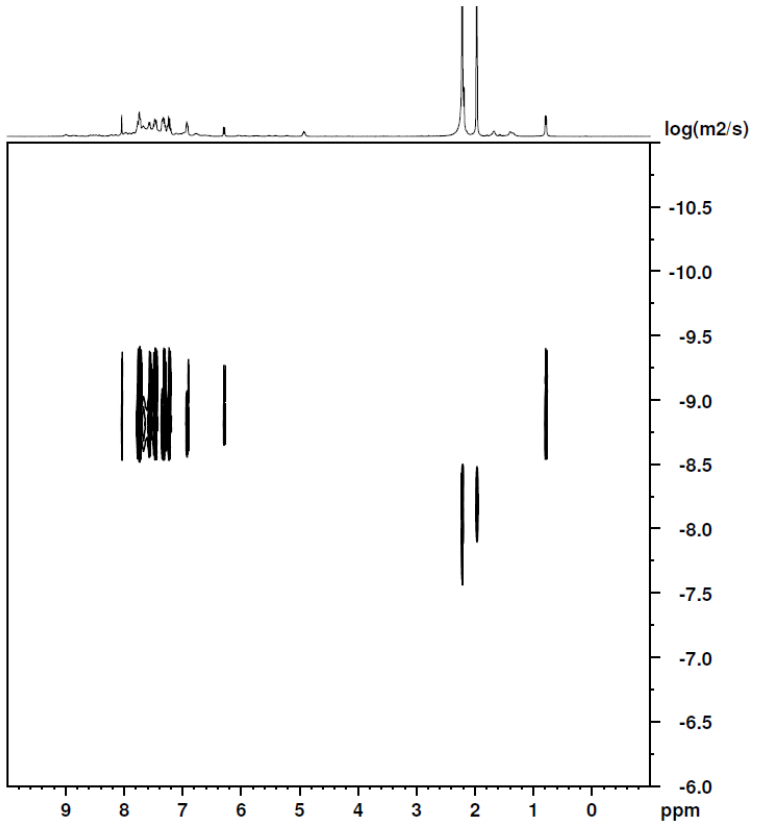

Fig. S15 ^{1}H DOSY spectrum of ***ΛΛ/ΔΔ*-La$_2$L$^{R/S}_3$** (D = 1.047×10^{-9} m^{2}s^{-1}, r = 6.07Å, 400 MHz, CD_3CN, 298 K).

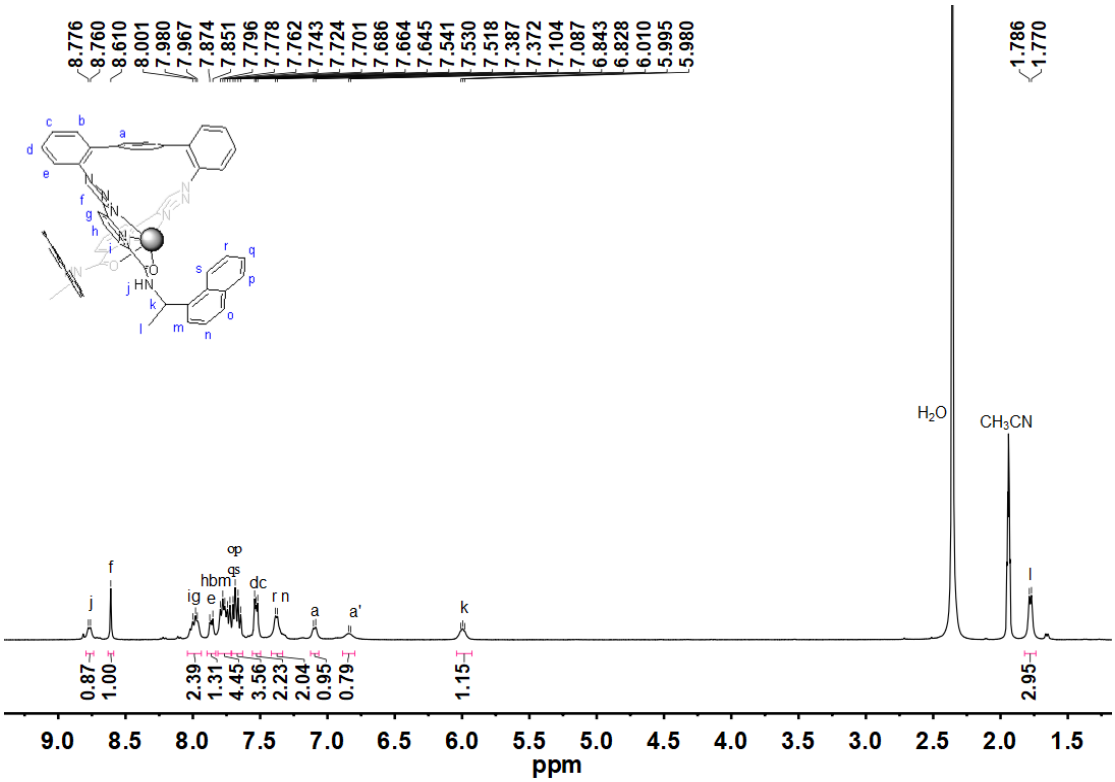

Fig. S16 ^{1}H NMR spectrum of ***Λ/Δ*-LaL$^{R/S}$** (400MHz, CD_3CN, 298K).

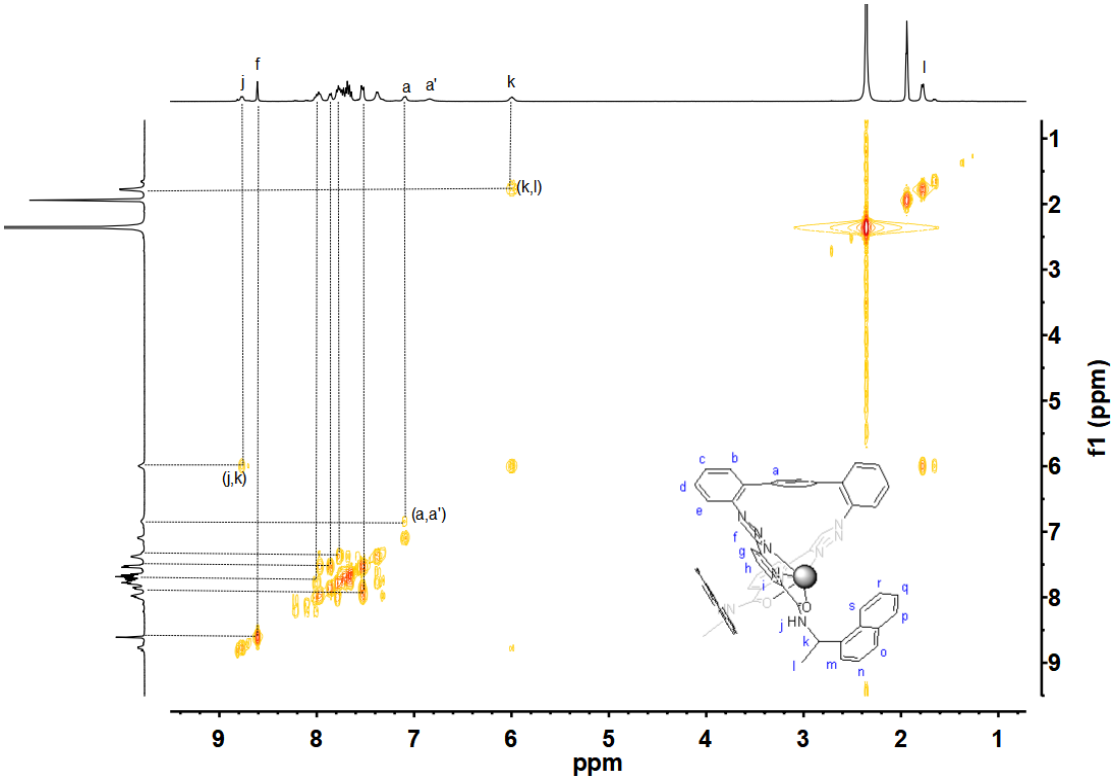

Fig. S17 ^{1}H-^{1}H COSY NMR spectrum of ***Λ/Δ*-LaL$^{R/S}$** (400 MHz, $CDCl_3$, 298 K).

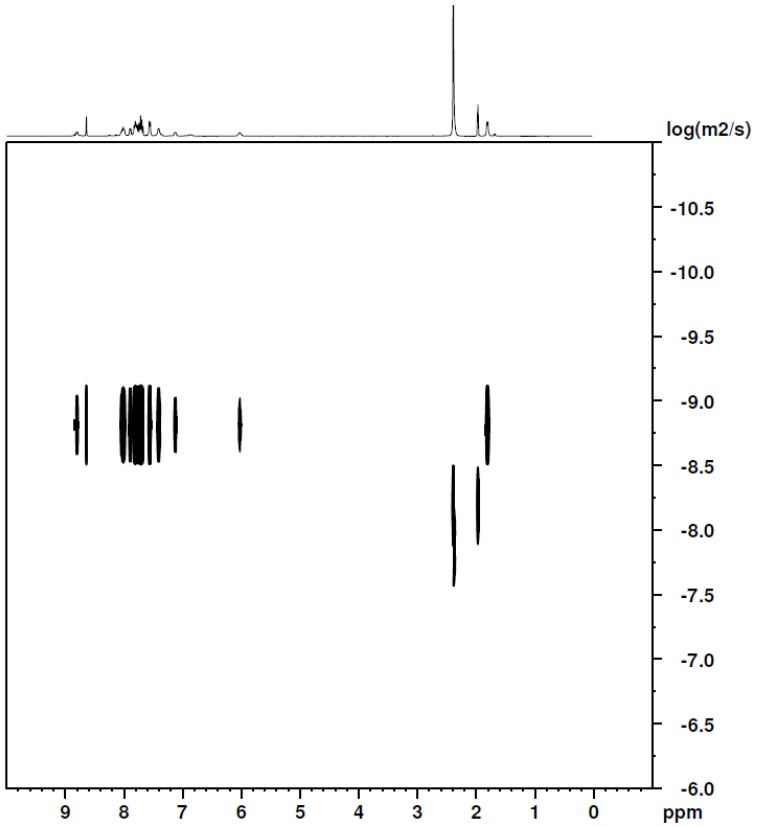

Fig. S18 ^{1}H DOSY spectrum of ***Λ/Δ*-LaL$^{R/S}$** (D=1.549×10^{-9} m^{2}s^{-1}, r = 4.11Å, 400 MHz, CD_3CN, 298 K).

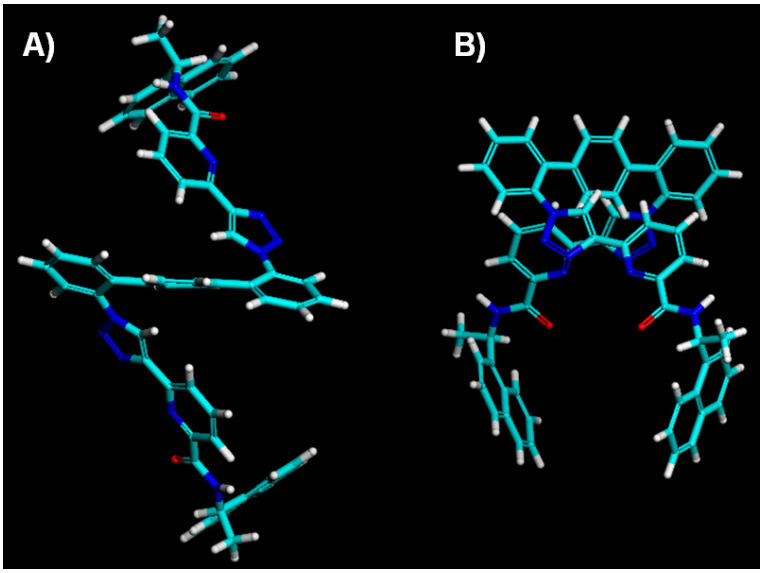

Fig. S19 The calculated optimal conformers of A) the *trans*-ligand and B) the *cis*-ligand with Materials Studio 6.0.

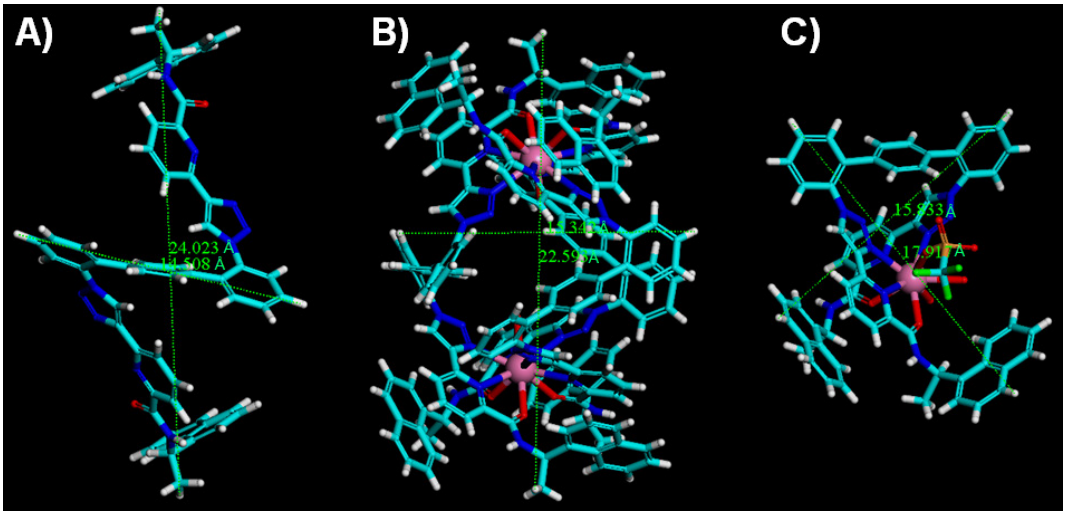

Fig. S20 The calculated optimal conformers of A) the *trans*-ligand and the compared crystal structures of B) ***ΔΔ*-La$_2$L$^R_3$** and C) ***Δ*-LaL^R**. The measured sizes are bigger than the DOSY dynamic ones due to the Stokes-Einstein equation is built on the spherical and rigid models.

Table S1 Computational studies of the *trans*- and *cis*-ligand with Materials Studio 6.0

	trans-L (kcal/mol)	*cis*-L (kcal/mol)
Total energy:	1293.264975	1320.230749
Valence energy (diag. terms):	1197.569	1193.367
Bond	1092.353	1091.588
Angle	85.829	86.008
Torsion	19.015	15.543
Inversion	0.371	0.229
Non-bond energy:	95.696	126.863
Van der Waals	95.696	126.863
Electrostatic	0.000	0.000

Molecular mechanic modelling suggest that the *trans*-conformer of the ligand is much more stable than the *cis*-ligand (Fig. S19, S20 and Table S1), giving rise to the dominated distribution of the trans-conformer for the ligand in solution, which explain why the diffusion coefficient of free ligand is significantly smaller than the mononuclear complex and similar with the helicate.

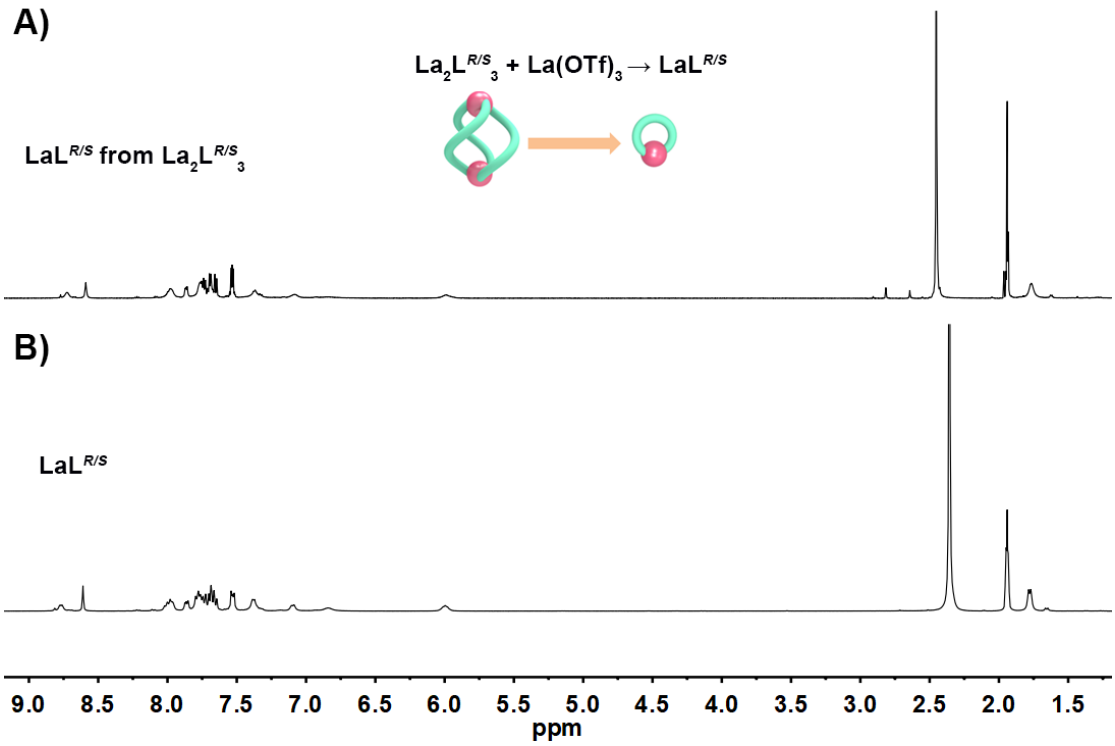

Fig. S21 ^{1}H NMR spectra of A) **LaL**$^{R/S}$ transformed from **La$_2$L**$^{R/S}_3$ and B) the compared **LaL**$^{R/S}$ (400MHz, CD_3CN, 298K).

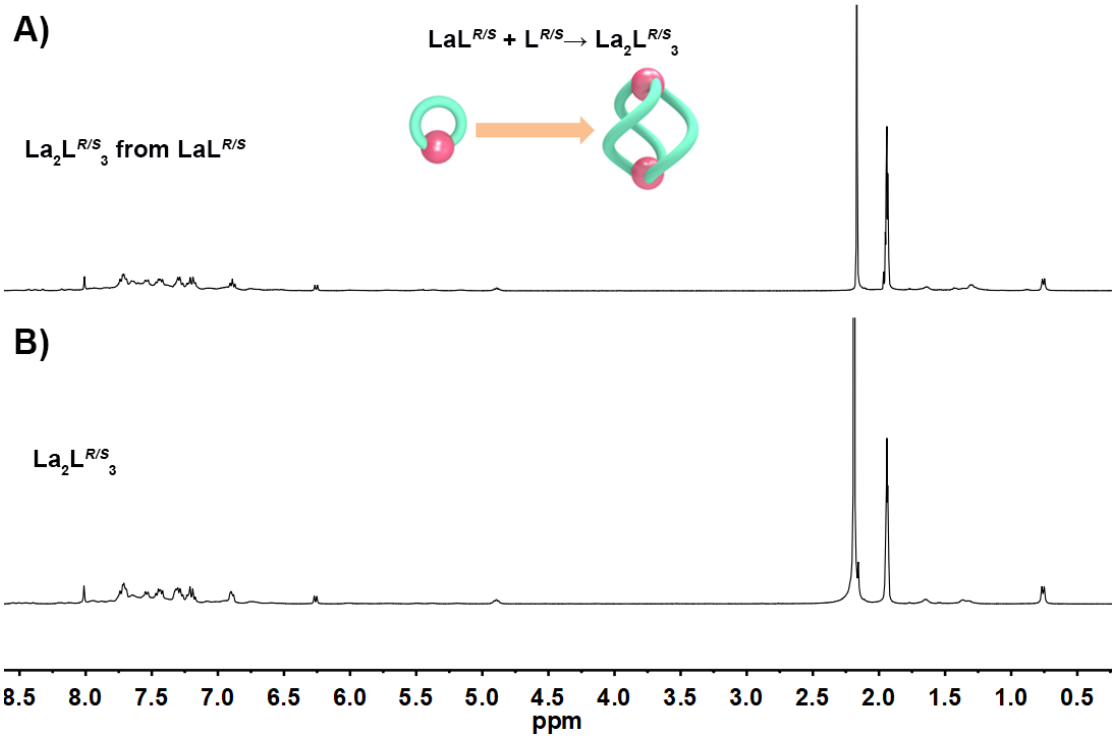

Fig. S22 ^{1}H NMR spectra of A) $\mathbf{La_2L^{R/S}_3}$ transformed from $\mathbf{LaL^{R/S}}$ and B) the compared $\mathbf{La_2L^{R/S}_3}$ (400MHz, CD_3CN, 298K).

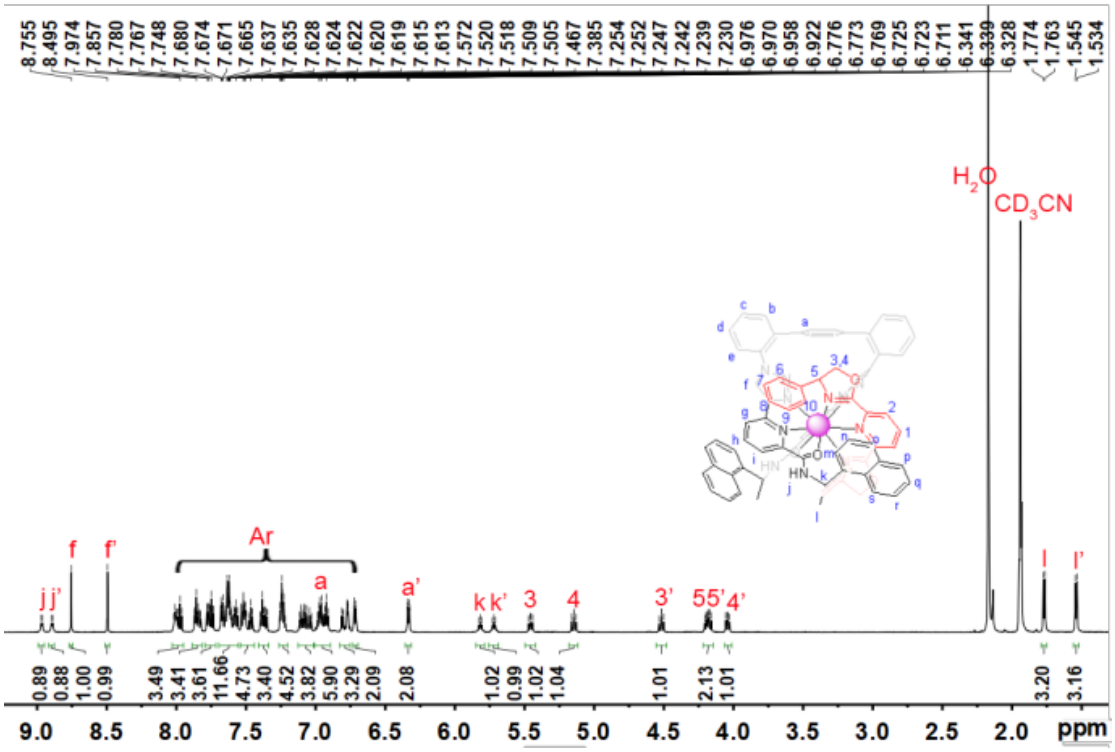

Fig. S23 ^{1}H NMR spectrum of $\mathbf{\Lambda}$**-LaL^{R}G^S** (400MHz, CD_3CN, 298K).

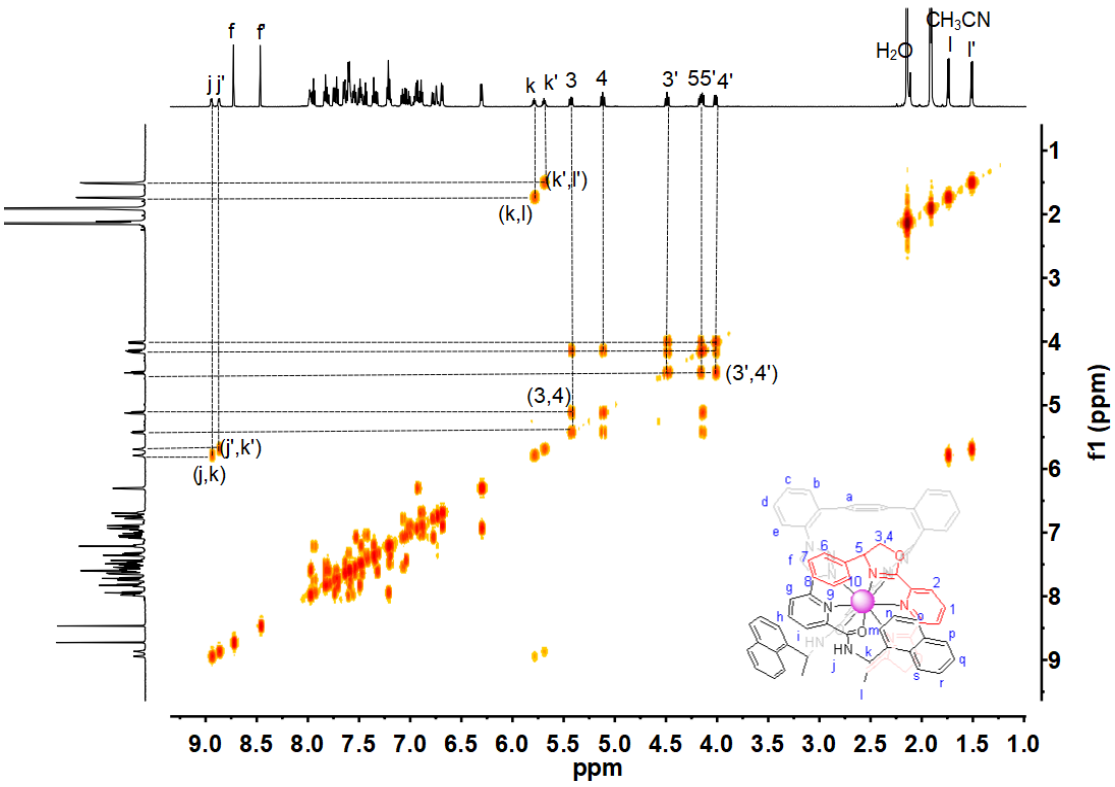

Fig. S24 ^{1}H-^{1}H COSY NMR spectrum of ***Λ*-LaL^{R}G^{S}** (400 MHz, $CDCl_3$, 298 K).

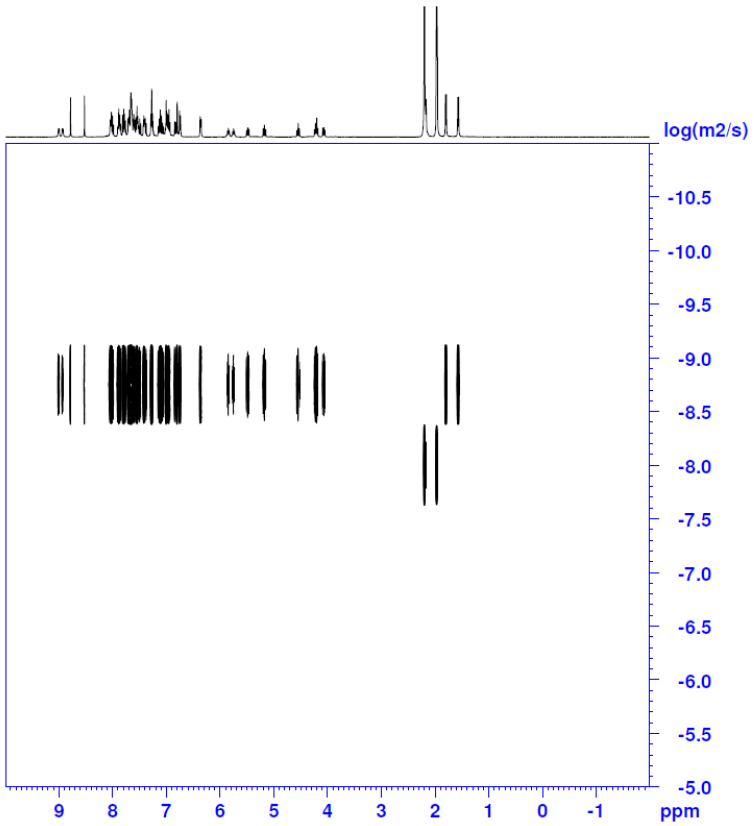

Fig. S25 ^{1}H DOSY spectrum of ***Λ*-LaL^{R}G^{S}** (D=1.778×10^{-9} m^{2}s^{-1}, r = 3.58Å, 400 MHz, CD_3CN, 298 K).

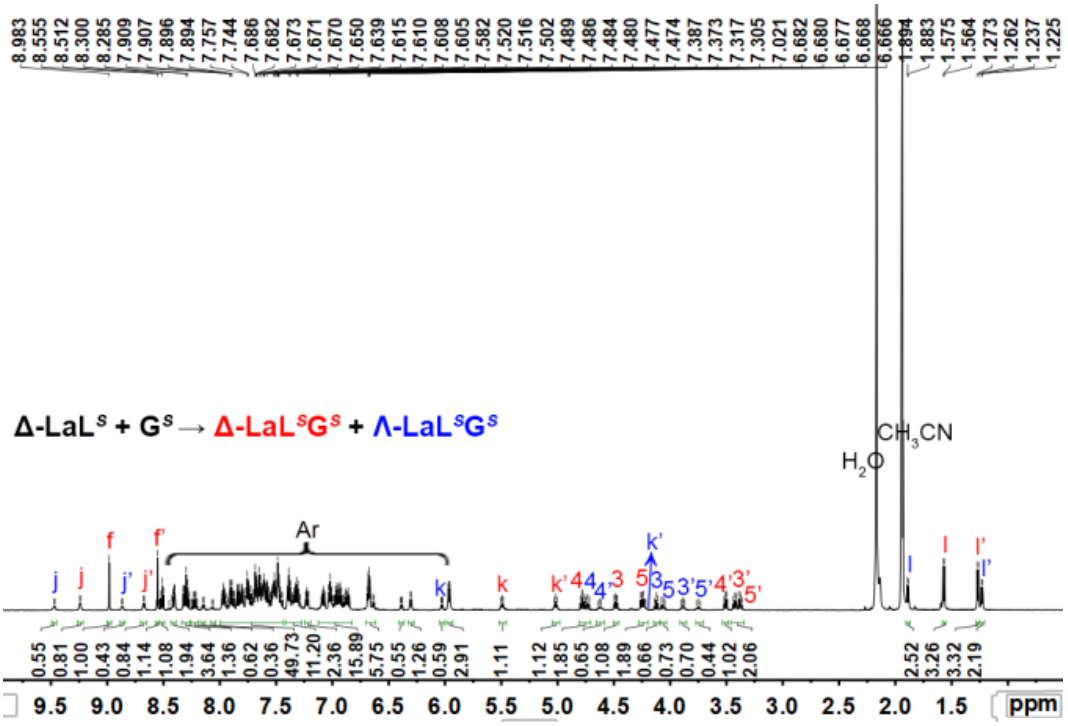

Fig. S26 ^{1}H NMR spectrum of ***Λ/Δ*-LaL^{S}G^{S}** (400MHz, CD_3CN, 298K).

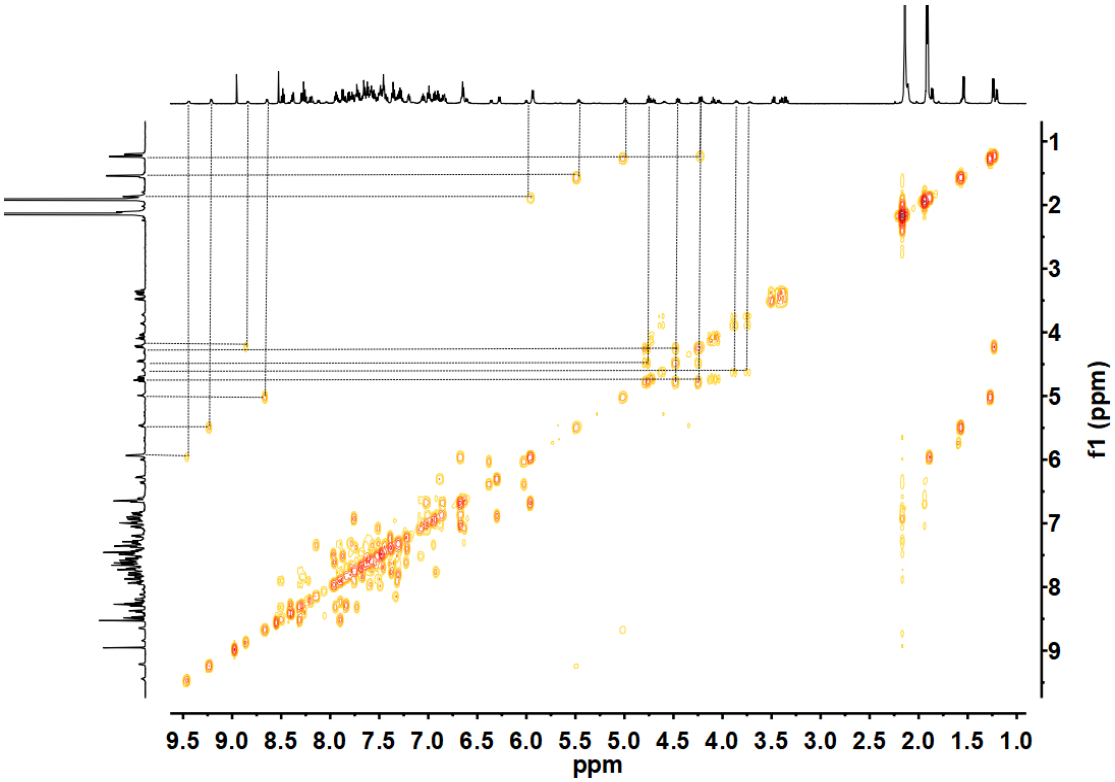

Fig. S27 ^{1}H-^{1}H COSY NMR spectrum of ***Λ/Δ*-LaL^{S}G^{S}** (400 MHz, $CDCl_3$, 298 K).

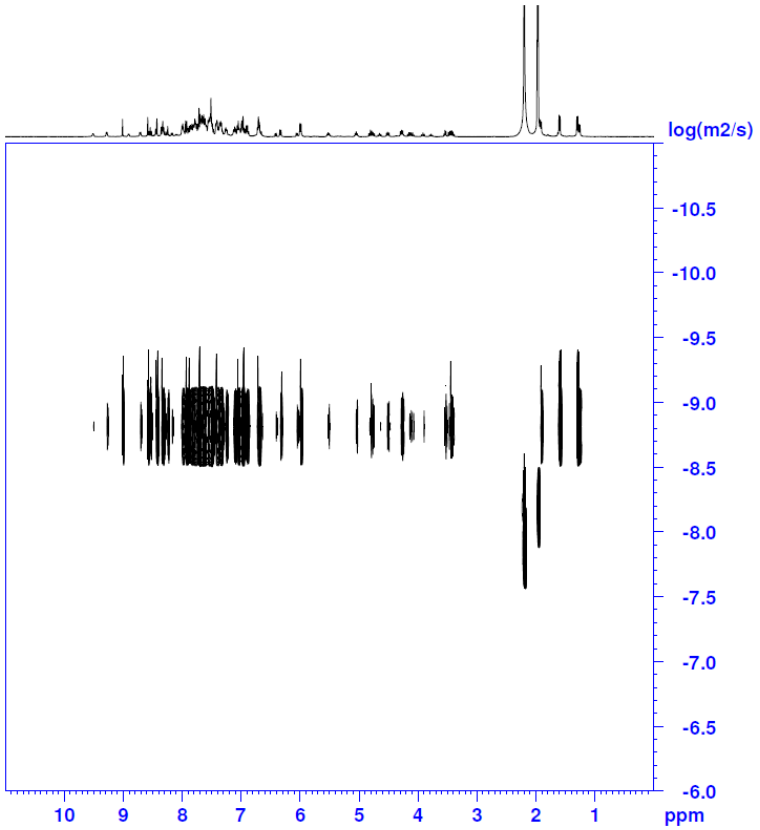

Fig. S28 ^{1}H DOSY spectrum of ***Λ/Δ*-LaL^{S}G^{S}** (D=1.514×10^{-9} m^{2}s^{-1}, r = 4.20Å, 400 MHz, CD_3CN, 298 K).

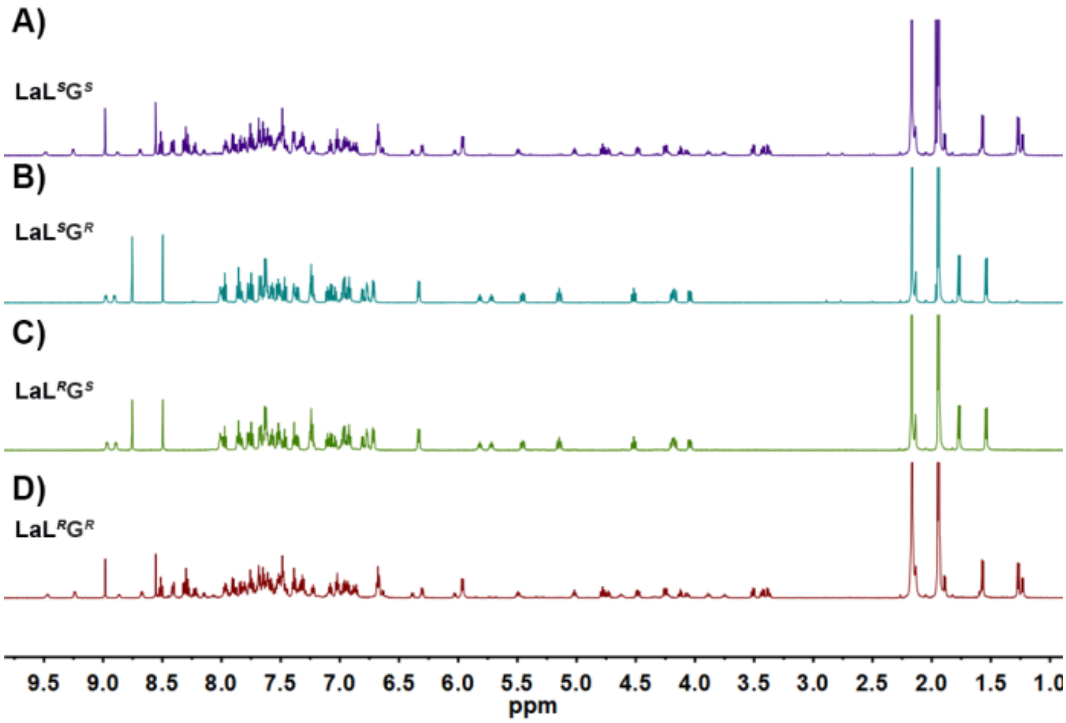

Fig. S29 ^{1}H NMR spectra(400MHz, CD_3CN, 298K) of A) **LaL^{S}G^{S}**, B) **LaL^{S}G^{R}**, C) **LaL^{R}G^{S}** and D) **LaL^{R}G^{R}**.

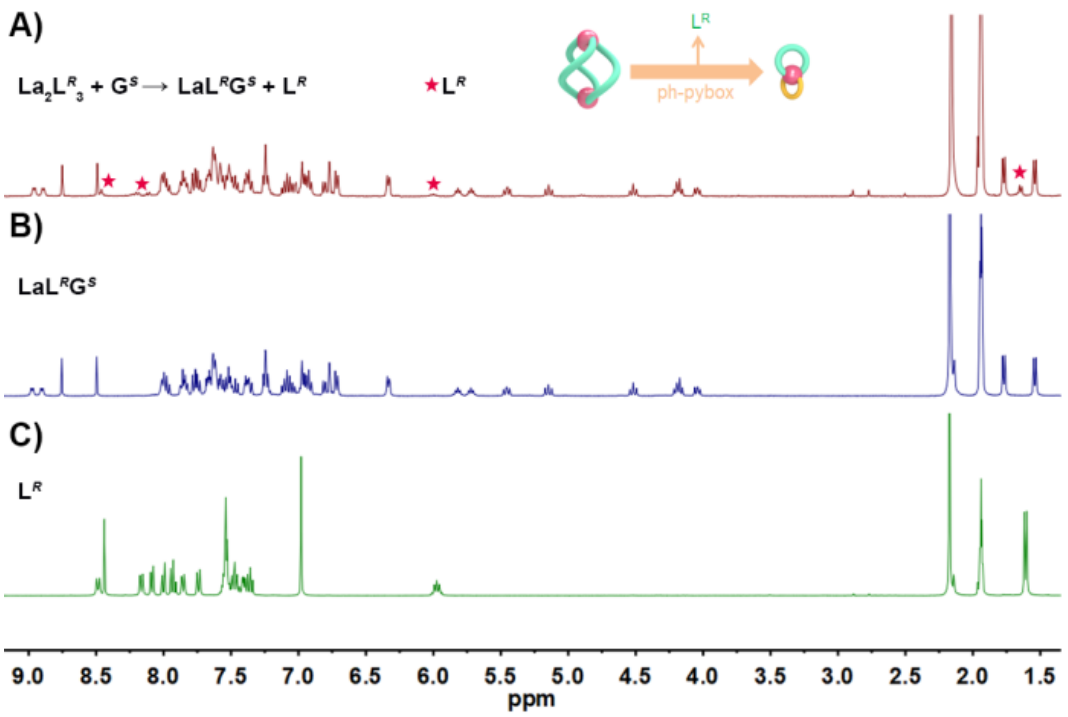

Fig. S30 ^{1}H NMR spectra (400MHz, CD_3CN, 298K) of A) $\mathbf{La_2L^R_3}$ added with 2eq $\mathbf{G^S}$ and the compared B) $\mathbf{LaL^RG^S}$, C) $\mathbf{L^R}$.

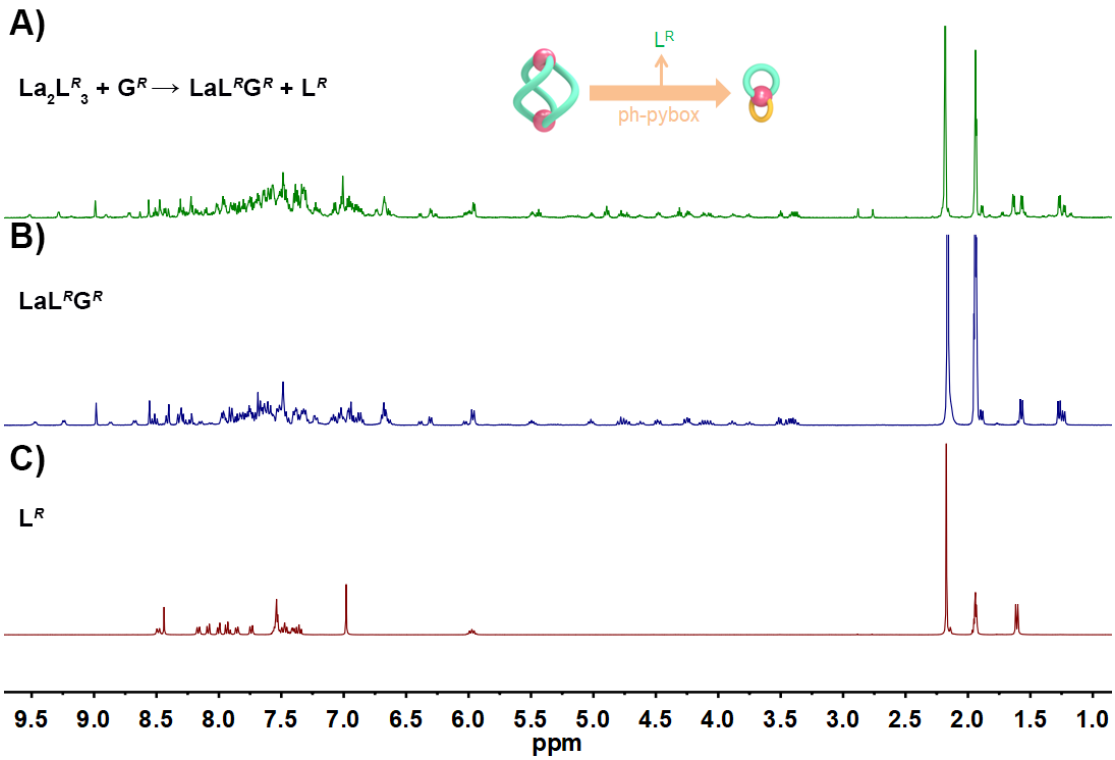

Fig. S31 ^{1}H NMR spectra (400MHz, CD_3CN, 298K) of A) $\mathbf{La_2L^R_3}$ added with 2eq $\mathbf{G^R}$ and the compared B) $\mathbf{LaL^RG^R}$, C) $\mathbf{L^R}$.

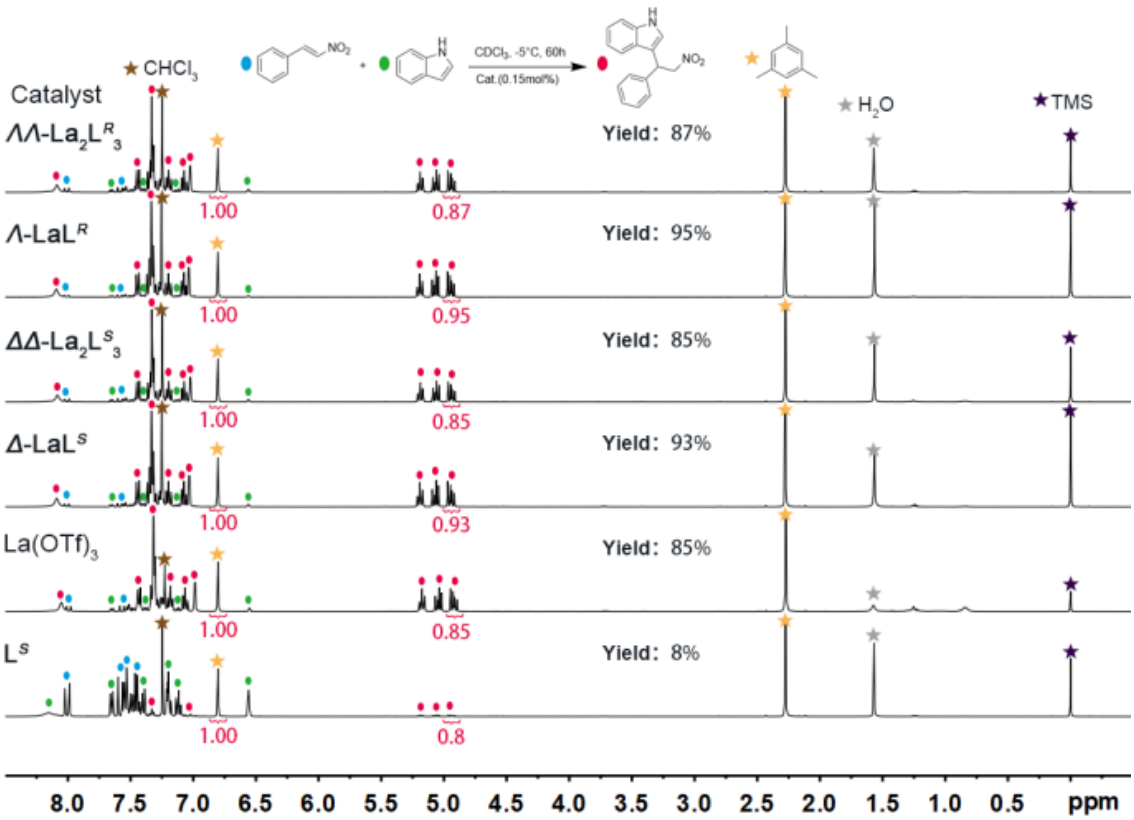

Fig. S32 ^{1}H NMR spectra (400 MHz, $CDCl_3$, 298 K) of the Friedel-Crafts products catalyzed by ***ΛΛ/ΔΔ*-La$_2$L$^{R/S}_3$**, ***Λ/Δ*-LaL$^{R/S}$**, La(OTf)$_3$ and L^{S}, respectively (-5℃,60 h, 0.15 mol% cat. loading). The signals of remained trans-β-nitrostyrene and indole were labeled as blue and green ovals, respectively. The signals of 3-(2-nitro-1-phenylethyl)-1H-indole were labeled as red ovals. 1,3,5-trimethylbenzene was used as internal standard substance and labeled as yellow pentacle. The yield were determined by the aromatic integral of 1,3,5-trimethylbenzene (0.33eq) and the methylene integral of product 3-(2-nitro-1-phenylethyl)-1H-indole.

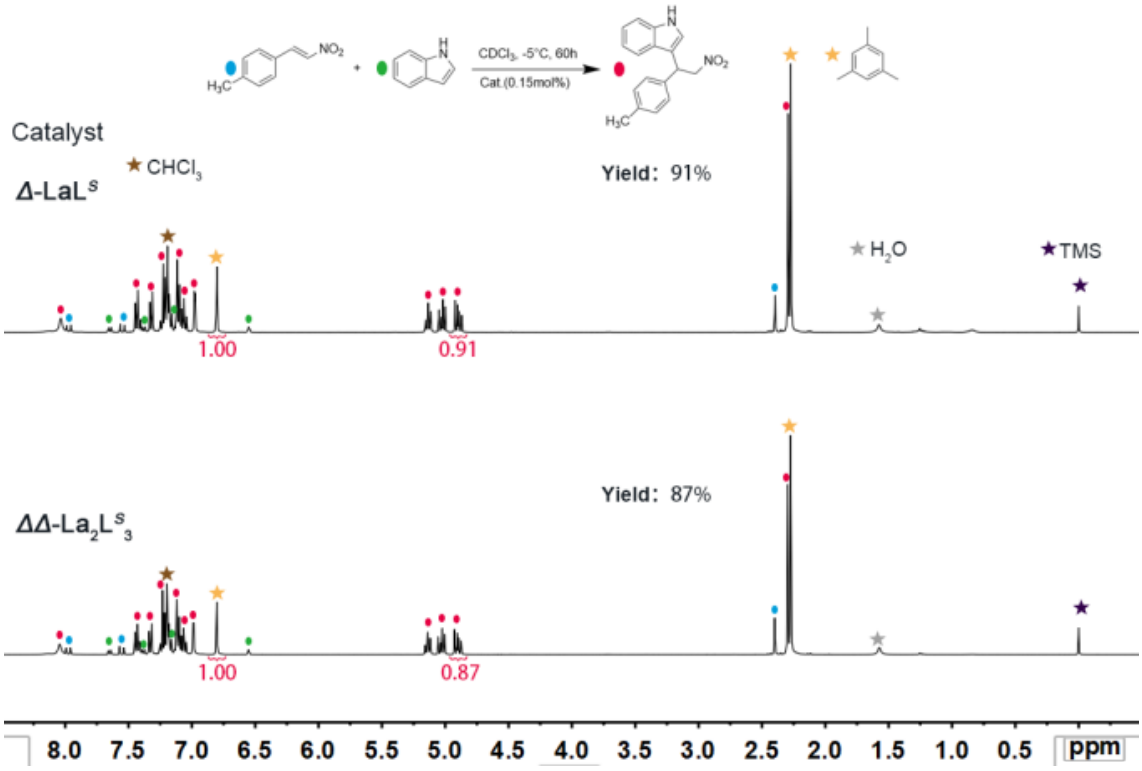

Fig. S33 ^{1}H NMR spectra (400 MHz, $CDCl_3$, 298 K) of the Friedel-Crafts products catalyzed by ***ΔΔ*-$La_2L^S_3$** and ***Δ*-LaL^S** (-5 ℃ ,60 h, 0.15 mol% cat. loading). The signals of remained (E)-1-methyl -4-(2-nitrovinyl)benzene and indole were labeled as blue and green ovals, respectively. The signals of 3-(2-nitro-1-(p-tolyl)ethyl)-1H-indole were labeled as red ovals. 1,3,5-trimethylbenzene was used as internal standard substance and labeled as yellow pentacle. The yield were determined by the aromatic integral of 1,3,5-trimethylbenzene (0.33eq) and the methylene integral of product 3-(2-nitro-1-(p-tolyl)ethyl)-1H-indole.

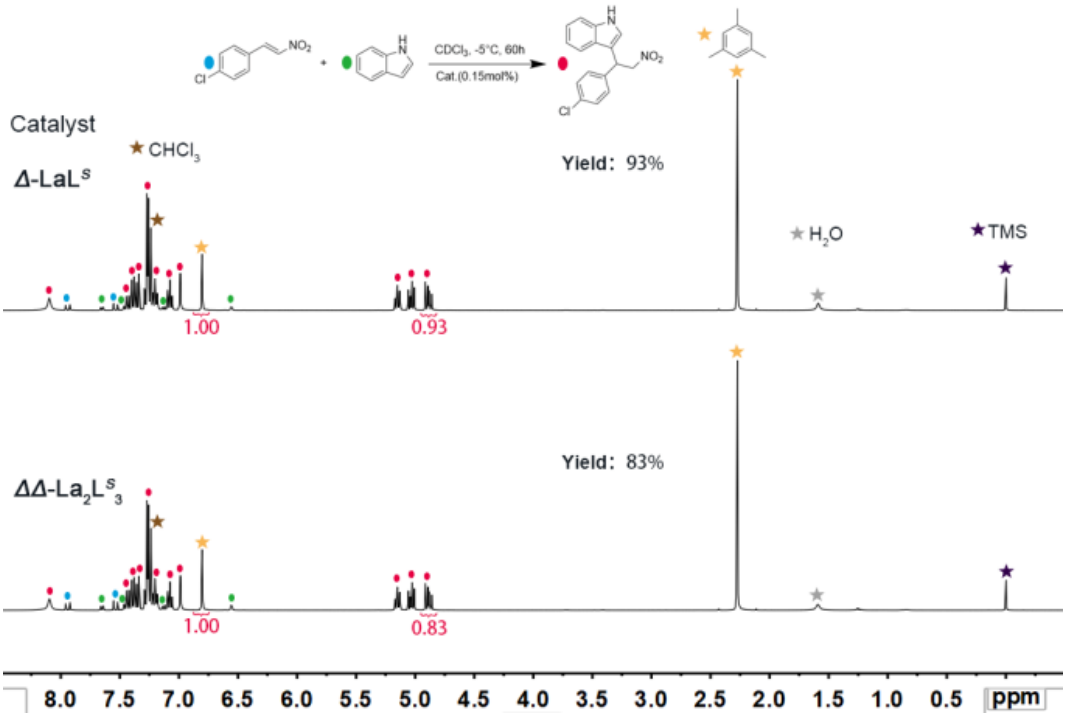

Fig. S34 ^{1}H NMR spectra (400 MHz, $CDCl_3$, 298 K) of the Friedel-Crafts products catalyzed by ***ΔΔ*-La$_2$L$^S_3$** and ***Δ*-LaL^S** (-5 ℃ ,60 h, 0.15 mol% cat. loading). The signals of remained (E)-1-chloro-4-(2-nitrovinyl)benzene and indole were labeled as blue and green ovals, respectively. The signals of 3-(1-(4-chlorophenyl)-2-nitroethyl)-1H-indole were labeled as red ovals. 1,3,5-trimethylbenzene was used as internal standard substance and labeled as yellow pentacle. The yield were determined by the aromatic integral of 1,3,5-trimethylbenzene (0.33eq) and the methylene integral of product 3-(1-(4-chlorophenyl)-2-nitroethyl)-1H-indole.

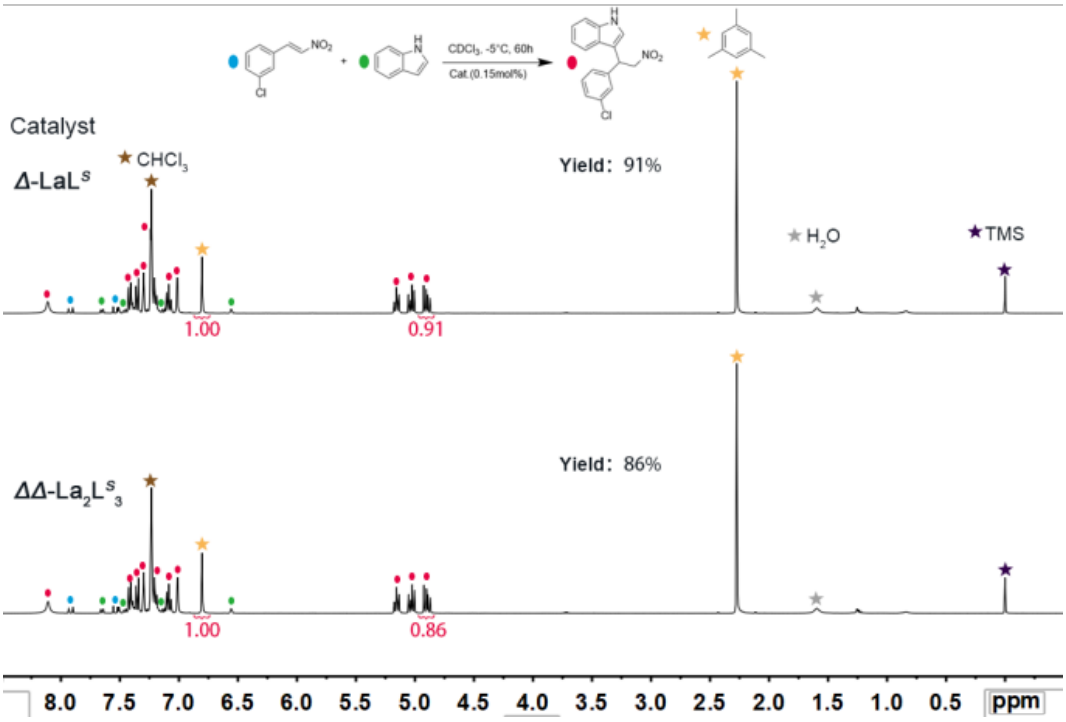

Fig. S35 ^{1}H NMR spectra (400 MHz, $CDCl_3$, 298 K) of the Friedel-Crafts products catalyzed by ***ΔΔ*-$La_2L^S_3$** and ***Δ*-LaL^S** (-5 ℃ ,60 h, 0.15 mol% cat. loading). The signals of remained (E)-1-chloro-3-(2-nitrovinyl)benzene and indole were labeled as blue and green ovals, respectively. The signals of 3-(1-(3-chlorophenyl)-2-nitroethyl)-1H-indole were labeled as red ovals. 1,3,5-trimethylbenzene was used as internal standard substance and labeled as yellow pentacle. The yield were determined by the aromatic integral of 1,3,5-trimethylbenzene (0.33eq) and the methylene integral of product 3-(1-(3-chlorophenyl)-2-nitroethyl)-1H-indole.

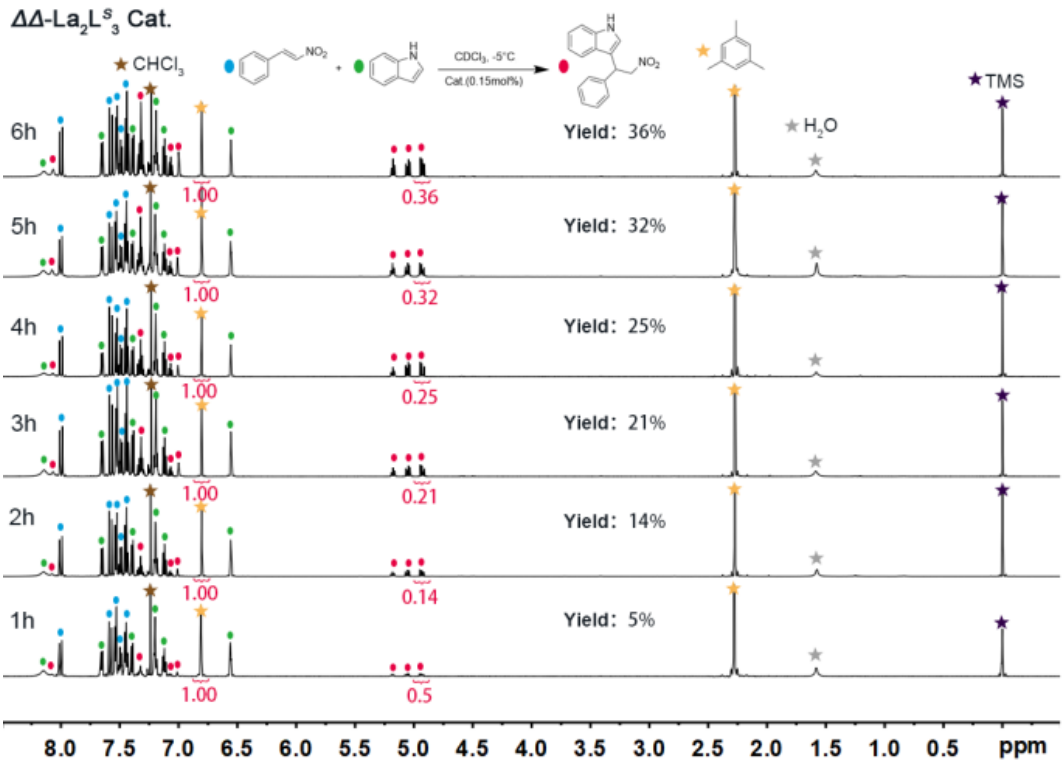

Fig. S36 ^{1}H NMR spectra (600 MHz, $CDCl_3$, 298 K) of the Friedel-Crafts products catalyzed by ***ΔΔ*-La$_2$L$^S_3$** (-5℃, 0.15mol% cat. loading) with different reaction time. The signals of remained trans-β-nitrostyrene and indole were labeled as blue and green ovals, respectively. The signals of 3-(2-nitro-1-phenylethyl)-1H-indole were labeled as red ovals. 1,3,5-trimethylbenzene was used as internal standard substance and labeled as yellow pentacle. The yield were determined by the aromatic integral of 1,3,5-trimethylbenzene (0.33eq) and the methylene integral of product 3-(2-nitro-1-phenylethyl)-1H-indole.

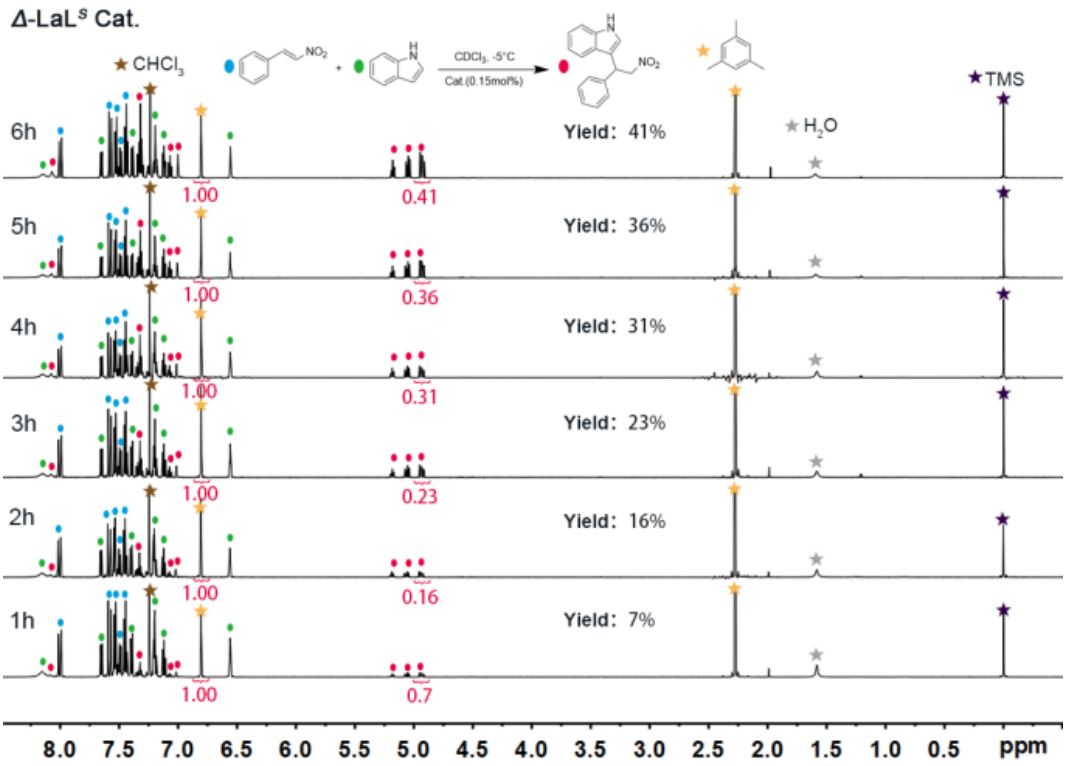

Fig. S37 ^{1}H NMR spectra (600 MHz, $CDCl_3$, 298 K) of the Friedel-Crafts products catalyzed by ***Δ*-LaL^S** (-5℃, 0.15 mol% cat. loading) with different reaction time. The signals of remained trans-β-nitrostyrene and indole were labeled as blue and green ovals, respectively. The signals of 3-(2-nitro-1-phenylethyl)-1H-indole were labeled as red ovals. 1,3,5-trimethylbenzene was used as internal standard substance and labeled as yellow pentacle. The yield were determined by the aromatic integral of 1,3,5-trimethylbenzene (0.33eq) and the methylene integral of product 3-(2-nitro-1-phenylethyl)-1H-indole.

Table S2. The original data of the kinetic study.

Time	$La_2L^S_3$-yield	LaL^S-yield	$La_2L^S_3$-1/(1-yield)	LaL^S-1/(1-yield)
0	0	0	1	1
1	0.05	0.07	1.05263	1.07527
2	0.14	0.16	1.16279	1.19048
3	0.21	0.23	1.26582	1.29870
4	0.25	0.31	1.33333	1.44928
5	0.32	0.36	1.47059	1.56250
6	0.36	0.41	1.56250	1.69492

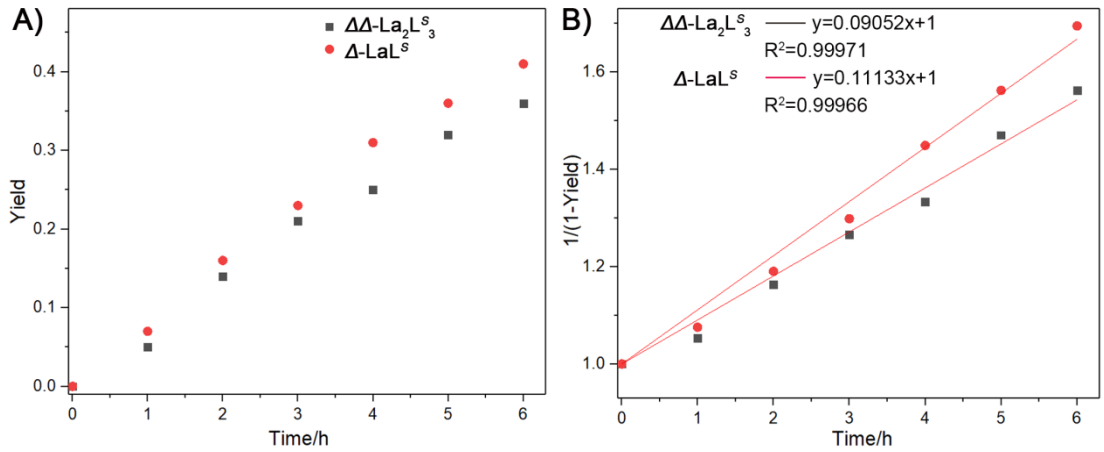

Fig. S38 A) Friedel-Crafts product yield plots for catalysts ***ΔΔ*-La$_2$L$^S_3$** (black) and ***Δ*-LaL^S** (red). B) Kinetic plots used to compare the second-order rate constants for the catalysts ***ΔΔ*-La$_2$L$^S_3$** (black) and ***Δ*-LaL^S** (red), respectively.

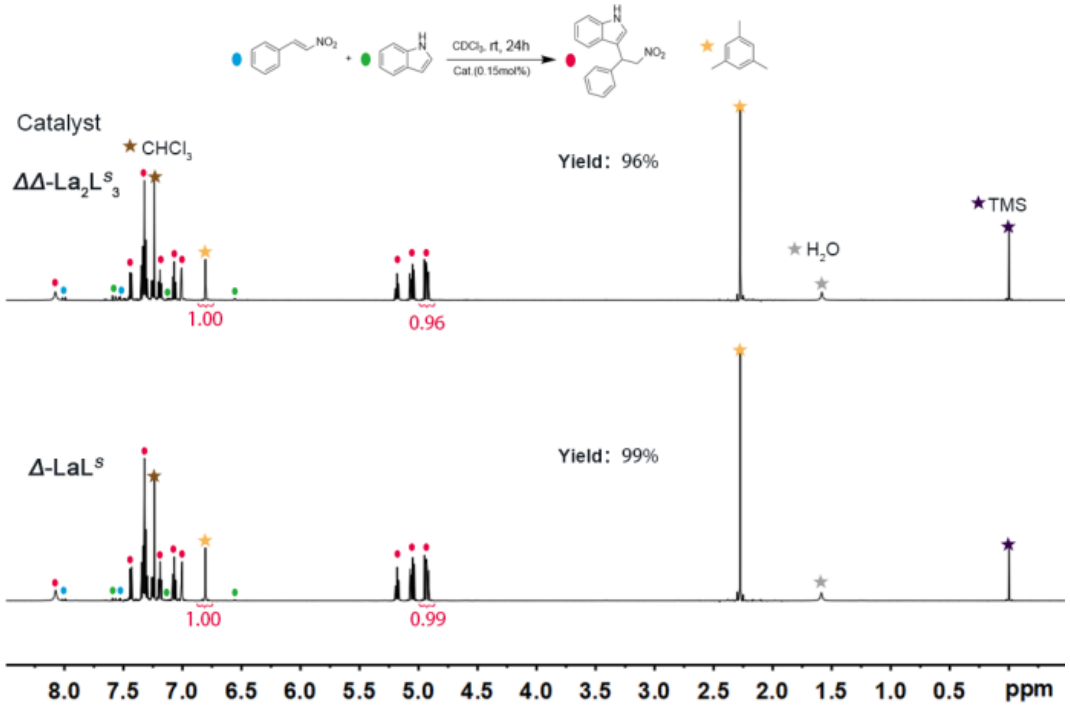

Fig. S39 ^{1}H NMR spectra (600 MHz, $CDCl_3$, 298 K) of the Friedel-Crafts crude products catalyzed by ***ΔΔ*-La$_2$L$^S_3$** and ***Δ*-LaL^S** (rt, 24 h, 0.15 mol% cat. loading). The signals of remained trans-β-nitrostyrene and indole were labeled as blue and green ovals, respectively. The signals of 3-(2-nitro-1-phenylethyl)-1H-indole were labeled as red ovals. 1,3,5-trimethylbenzene was used as internal standard substance and labeled as yellow pentacle. The yield were determined by the aromatic integral of 1,3,5-trimethylbenzene (0.33eq) and the methylene integral of product 3-(2-nitro-1-phenylethyl)-1H-indole.

4. ESI-TOF-MS analyses

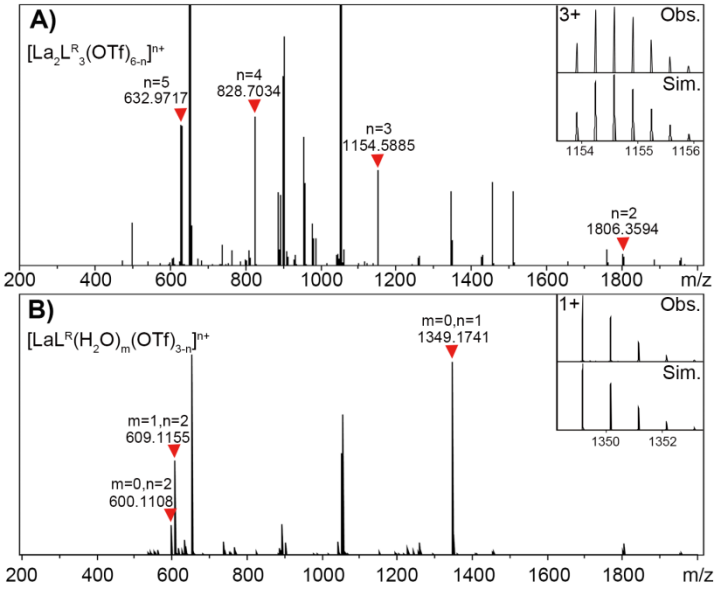

Fig. S40 ESI-TOF-MS spectra of A) ***ΛΛ*-$La_2L^R_3$** and B) ***Λ*-LaL^R**, with inserts showing the observed and simulated isotopic patterns of the peaks corresponding to $[(La_2L^R_3)(OTf)_3]^{3+}$ and $[(LaL^R)(OTf)_2]^+$.

The tandem mass spectrometry (MS/MS) experiments were carried out to confirm whether $La_2L^R_3$ decomposed in the gas-phase during MS measurement. The $[(La_2L^R_3)(OTf)_3]^{3+}$ ion (corresponding to m/z value of 1154.5845) was isolated and subjected to collisional activation with N_2 at collision energies ranging from 0 to 15 eV. Two new peaks at 1056.2887 and1349.1691, corresponding to $[(LaL^R_2)(OTf)]^{2+}$ and $[(LaL^R)(OTf)_2]^+$, respectively, were detected expressly even no collision energy exerted. Along with the collision energy gradually increased to 15 eV, the chosen $[(La_2L^R_3)(OTf)_3]^{3+}$ ion was completely dissociated into $[(LaL^R_2)(OTf)]^{2+}$ and $[(LaL^R)(OTf)_2]^+$. Hence, we attributed the two species of LaL^R_2 and LaL^R to the decomposition of the dinuclear complex ***ΛΛ*-$La_2L^R_3$** in the gas-phase during MS measurement.

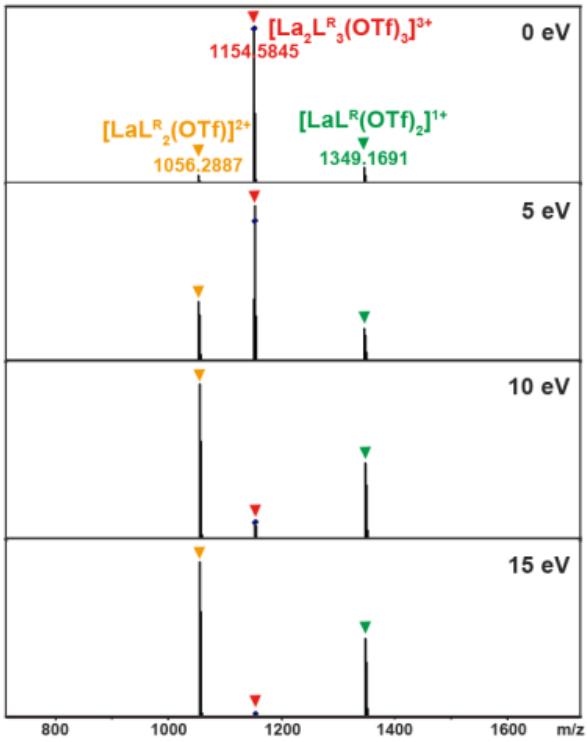

Fig. S41 Gradient tandem mass spectrometry (MS/MS) of $[(La_2L^R_3)(OTf)_3]^{3+}$ (m/z = 1154.5845) with various collision energies (from 0 V until total disassociation of the complex). Fragment peaks were assigned to the $[(LaL^R)(OTf)]^{2+}$ and $[(LaL^R)(OTf)_2]^{+}$.

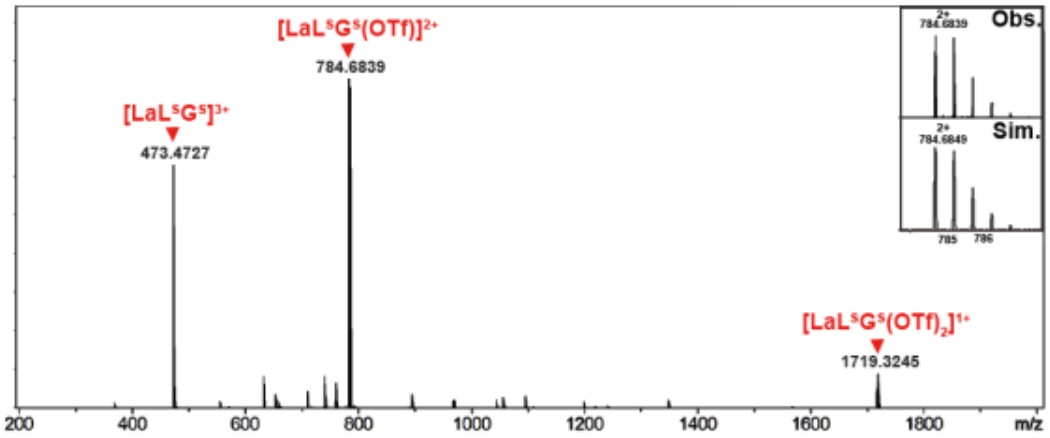

Fig. S42 ESI-TOF-MS spectra of **LaL^{S}G^S**, with inserts showing the observed and simulated isotopic patterns of the peaks corresponding to $[(LaL^SG^S)(OTf)]^{2+}$.

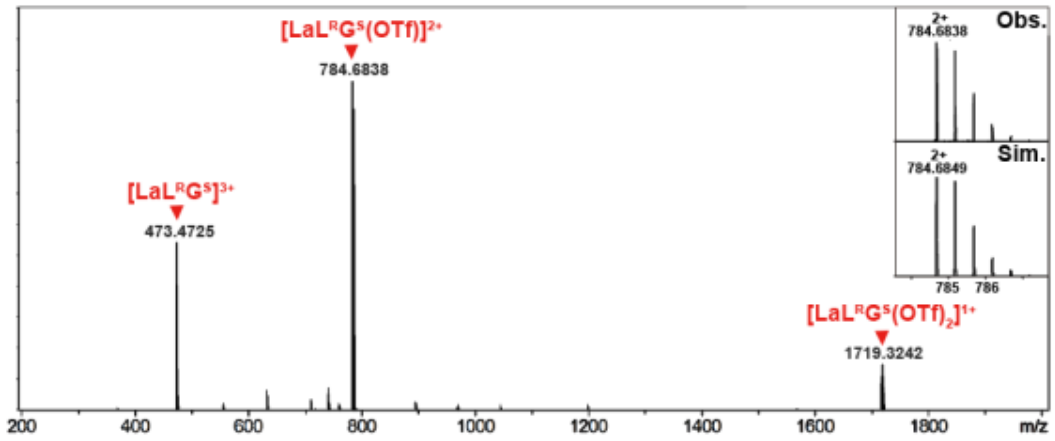

Fig. S43 ESI-TOF-MS spectra of $\mathbf{LaL^{\mathit{R}}G^{\mathit{S}}}$, with inserts showing the observed and simulated isotopic patterns of the peaks corresponding to $[(LaL^{R}G^{S})(OTf)]^{2+}$.

5. CD analyses

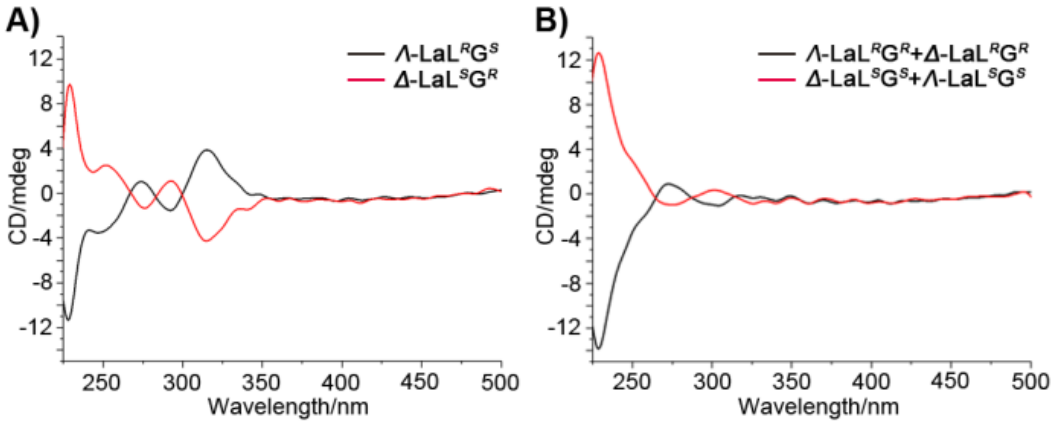

Fig. S44 CD spectra of A) $\mathbf{\Lambda/\Delta\text{-}LaL^{R/S}G^{S/R}}$ (1×10^{-5}M) and B) $\mathbf{\Lambda\text{-}LaL^{R}G^{R}}$ +$\mathbf{\Delta\text{-}LaL^{R}G^{R}}$ and $\mathbf{\Delta\text{-}LaL^{S}G^{S}}$ +$\mathbf{\Lambda\text{-}LaL^{S}G^{S}}$ (1×10^{-5}M) in CH_3CN. The remained metal-centered CD peaks at about 323 nm in B) illustrate the reversed chirality by $\mathbf{G^{R/S}}$ is in the minority.

6. HPLC analyses

All the spectra were performed by HPLC on chiral AD-H column (hexane/2-propanol 90:10, 0.8 ml/min, UV = 254 nm).

<Chromatogram>

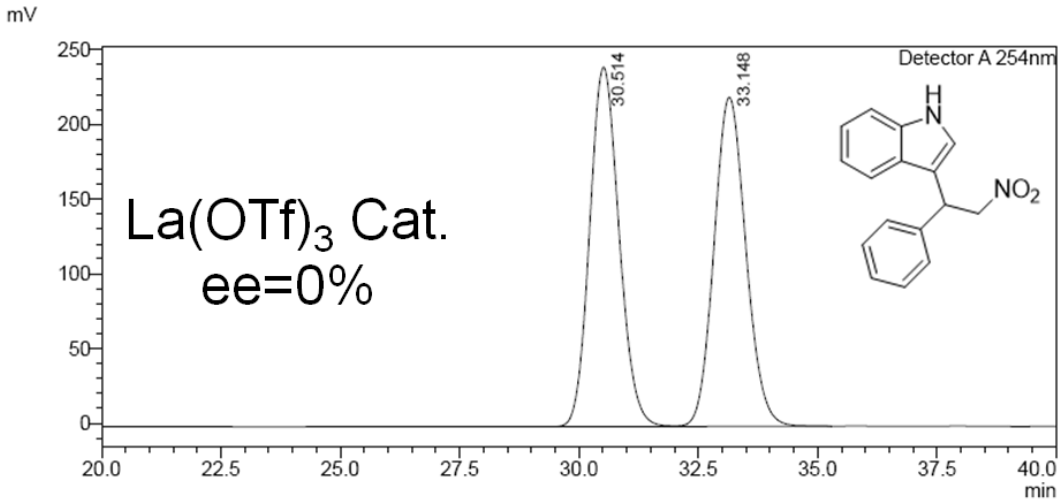

<Peak Table>

Detector A 254nm

Peak#	Ret. Time	Area	Height	Conc.	Unit	Mark	Name
1	30.514	10288803	240372	50.147			
2	33.148	10228585	220096	49.853		V	
Total		20517388	460468				

Fig. S45 HPLC spectrum of the Friedel-Crafts product 3-(2-nitro-1-phenylethyl)-1H-indole catalyzed by $La(OTf)_3$.

<Chromatogram>

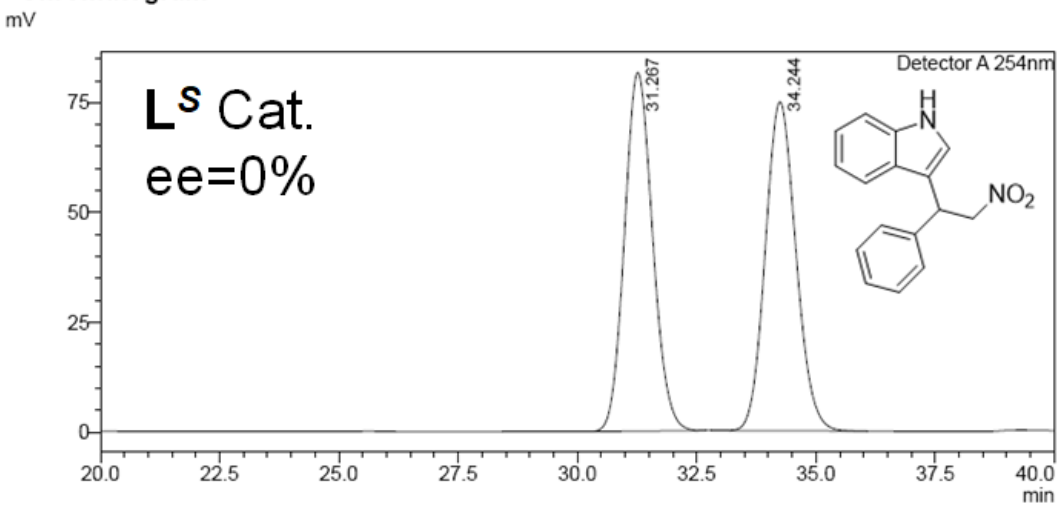

<Peak Table>

Detector A 254nm

Peak#	Ret. Time	Area	Height	Conc.	Unit	Mark	Name
1	31.267	3348620	81588	49.994			
2	34.244	3349478	74784	50.006			
Total		6698097	156371				

Fig. S46 HPLC spectrum of the Friedel-Crafts product 3-(2-nitro-1-phenylethyl)-1H-indole catalyzed by $\mathbf{L}^{S}$.

<Chromatogram>

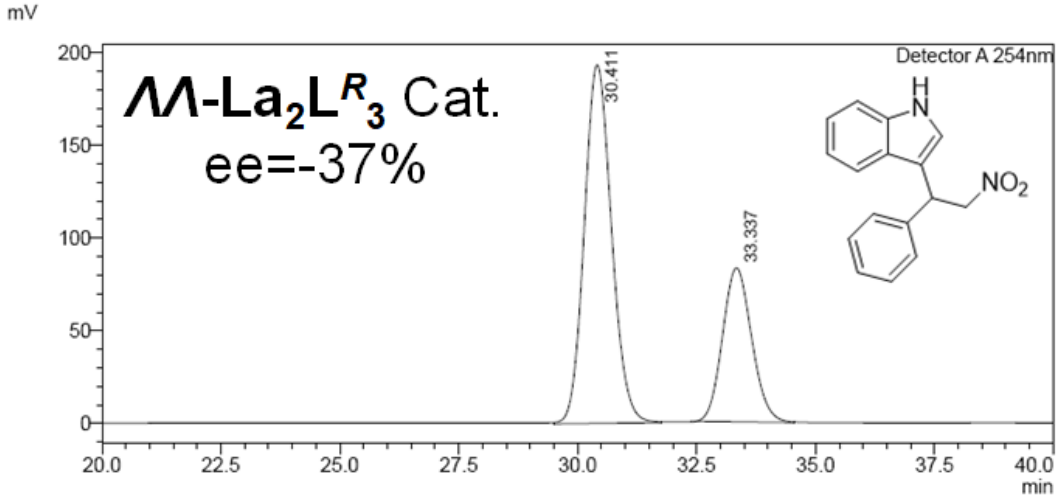

<Peak Table>

Detector A 254nm

Peak#	Ret. Time	Area	Height	Conc.	Unit	Mark	Name
1	30.411	7706684	193346	68.534		M	
2	33.337	3538311	82995	31.466		M	
Total		11244995	276341				

Fig. S47 HPLC spectrum of the Friedel-Crafts product 3-(2-nitro-1-phenylethyl)-1H-indole catalyzed by ***ΛΛ*-La$_2$L$^R_3$**.

<Chromatogram>

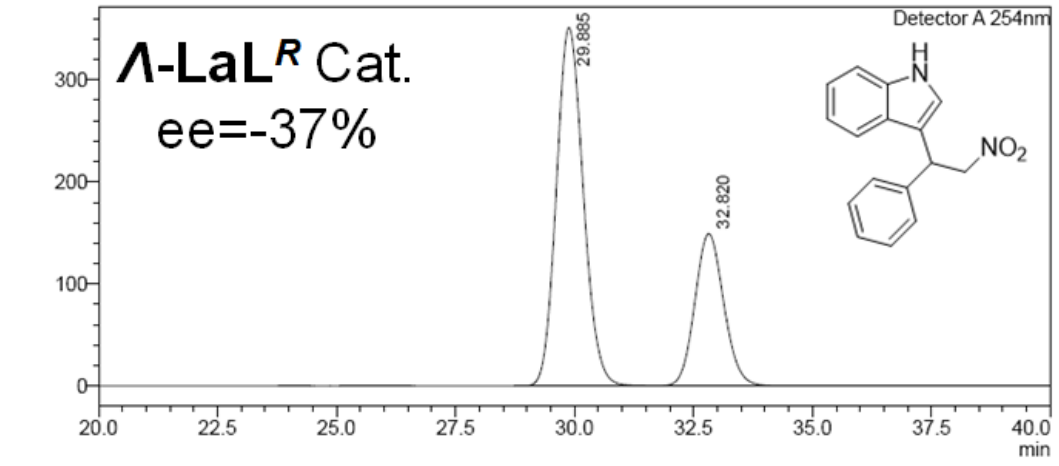

<Peak Table>

Detector A 254nm

Peak#	Ret. Time	Area	Height	Conc.	Unit	Mark	Name
1	29.885	13838246	351188	68.678			
2	32.820	6311150	149043	31.322		V	
Total		20149396	500231				

Fig. S48 HPLC spectrum of the Friedel-Crafts product 3-(2-nitro-1-phenylethyl)-1H-indole catalyzed by ***Λ*-LaL^R**.

<Chromatogram>

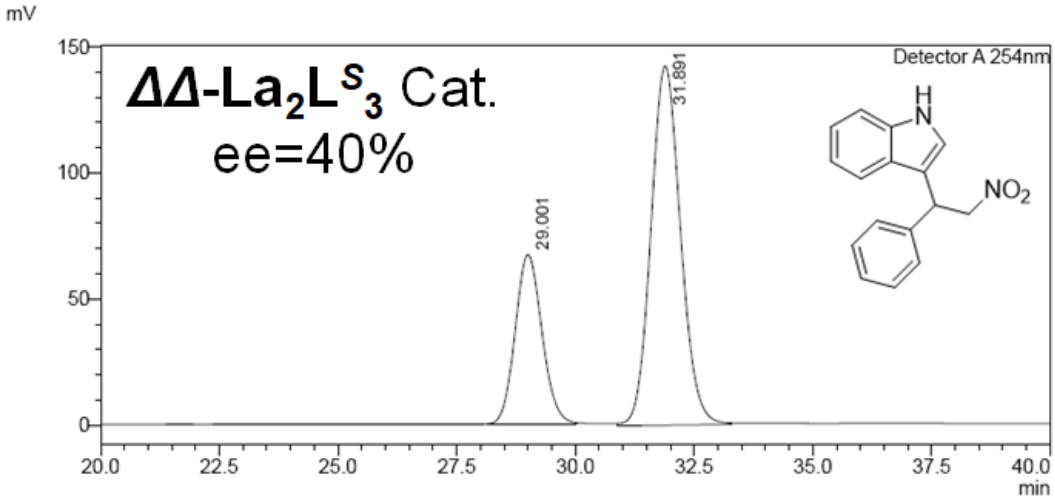

<Peak Table>

Detector A 254nm

Peak#	Ret. Time	Area	Height	Conc.	Unit	Mark	Name
1	29.001	2649931	67244	30.024		M	
2	31.891	6176023	142320	69.976		M	
Total		8825955	209565				

Fig. S49 HPLC spectrum of the Friedel-Crafts product 3-(2-nitro-1-phenylethyl)-1H-indole catalyzed by ***ΔΔ*-La$_2$L$^S_3$**.

<Chromatogram>

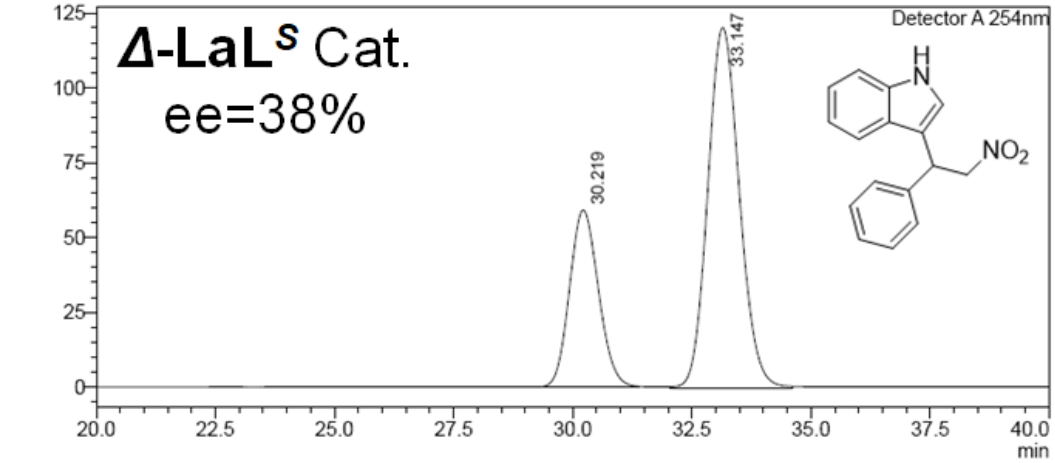

<Peak Table>

Detector A 254nm

Peak#	Ret. Time	Area	Height	Conc.	Unit	Mark	Name
1	30.219	2489192	59041	30.923		M	
2	33.147	5560371	120376	69.077		M	
Total		8049563	179416				

Fig. S50 HPLC spectrum of the Friedel-Crafts product 3-(2-nitro-1-phenylethyl)-1H-indole catalyzed by ***Δ*-LaL^S**.

<Chromatogram>

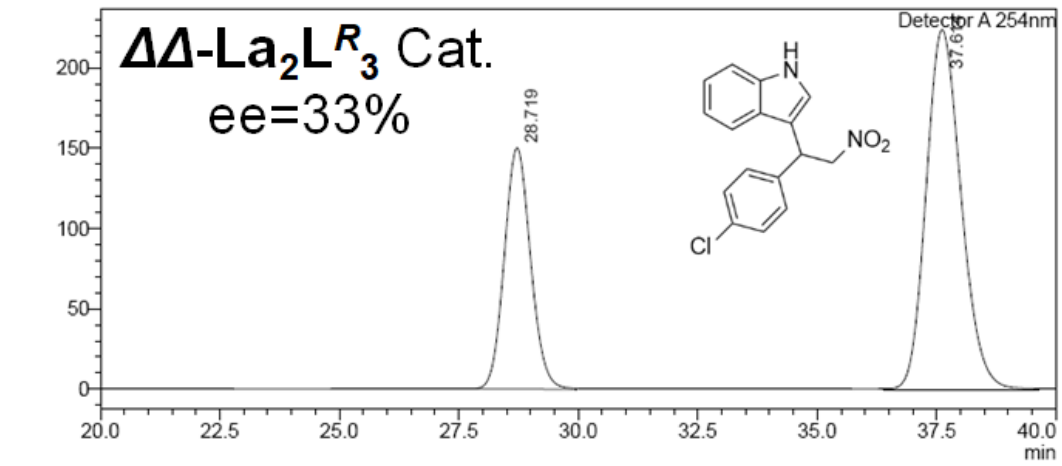

<Peak Table>

Detector A 254nm

Peak#	Ret. Time	Area	Height	Conc.	Unit	Mark	Name
1	28.719	5751069	150072	33.518		M	
2	37.614	11407275	223882	66.482		M	
Total		17158344	373954				

Fig. S51 HPLC spectrum of the Friedel-Crafts product 3-(1-(4-chlorophenyl)-2-nitroethyl)-1H-indole catalyzed by ***ΔΔ*-La$_2$L$^S_3$**.

<Chromatogram>

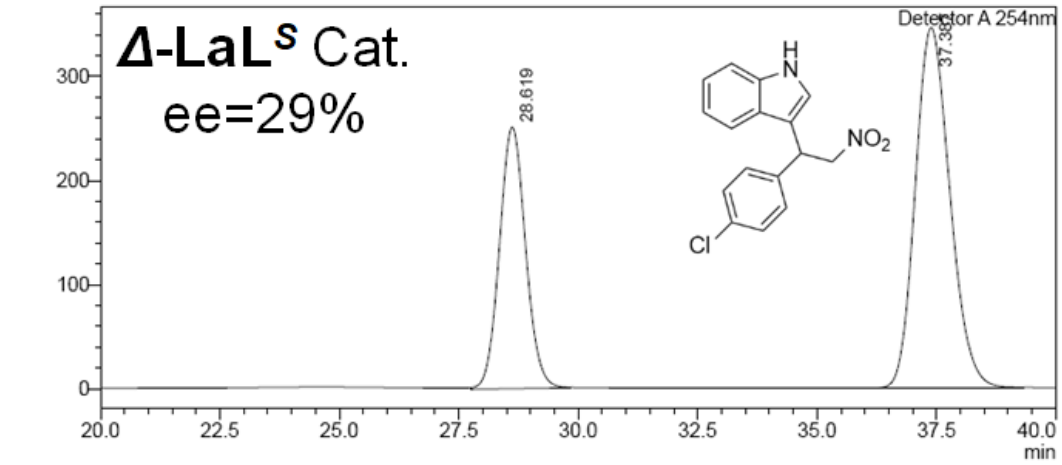

<Peak Table>

Detector A 254nm

Peak#	Ret. Time	Area	Height	Conc.	Unit	Mark	Name
1	28.619	9562998	250875	35.411		M	
2	37.387	17442548	345814	64.589		M	
Total		27005546	596689				

Fig. S52 HPLC spectrum of the Friedel-Crafts product 3-(1-(4-chlorophenyl)-2-nitroethyl)-1H-indole catalyzed by ***Δ*-LaL^S**.

<Chromatogram>

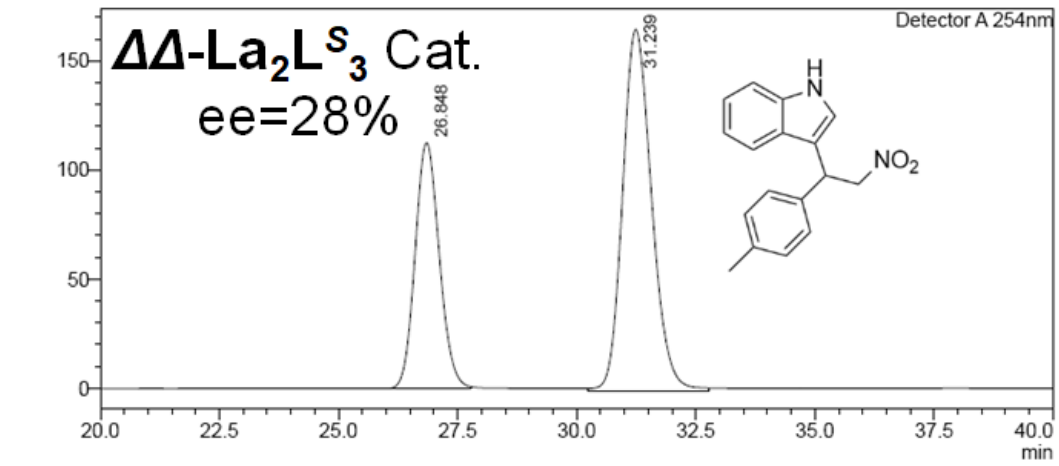

<Peak Table>

Detector A 254nm

Peak#	Ret. Time	Area	Height	Conc.	Unit	Mark	Name
1	26.848	3988453	112628	36.257		M	
2	31.239	7011908	165478	63.743		M	
Total		11000361	278106				

Fig. S53 HPLC spectrum of the Friedel-Crafts product 3-(2-nitro-1-(p-tolyl)ethyl)-1H-indole catalyzed by ***ΔΔ*-La$_2$L$^S_3$**.

<Chromatogram>

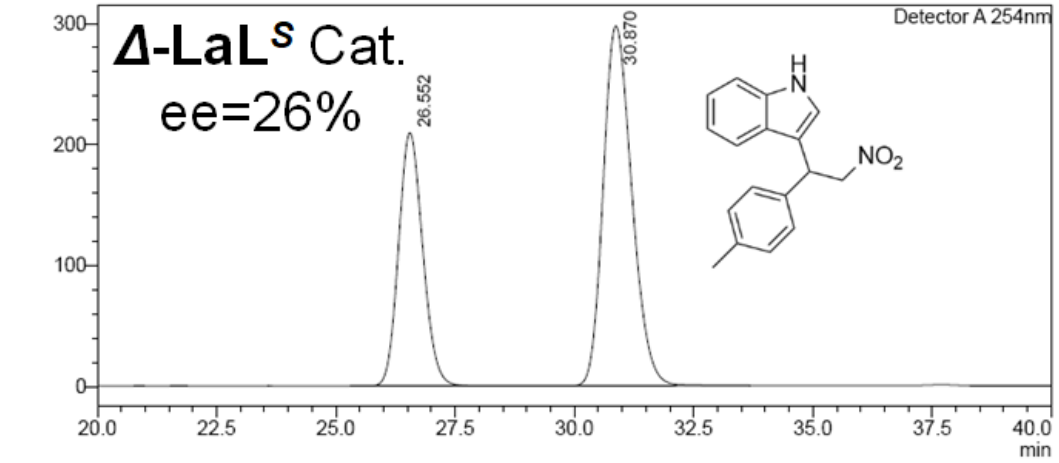

<Peak Table>

Detector A 254nm

Peak#	Ret. Time	Area	Height	Conc.	Unit	Mark	Name
1	26.552	7381397	209332	37.263			
2	30.870	12427538	297404	62.737			
Total		19808935	506736				

Fig. S54 HPLC spectrum of the Friedel-Crafts product 3-(2-nitro-1-(p-tolyl)ethyl)-1H-indole catalyzed by ***Δ*-LaL^S**.

<Chromatogram>

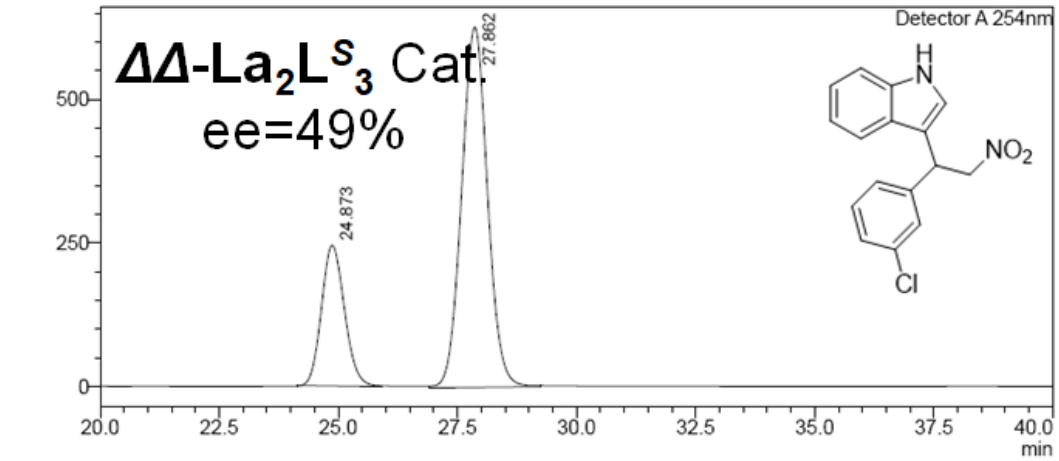

<Peak Table>

Detector A 254nm

Peak#	Ret. Time	Area	Height	Conc.	Unit	Mark	Name
1	24.873	8217647	244728	25.719		M	
2	27.862	23734329	627660	74.281		M	
Total		31951976	872388				

Fig. S55 HPLC spectrum of the Friedel-Crafts product 3-(1-(3-chlorophenyl)-2-nitroethyl)-1H-indole catalyzed by ***ΔΔ*-La$_2$L$^S_3$**.

<Chromatogram>

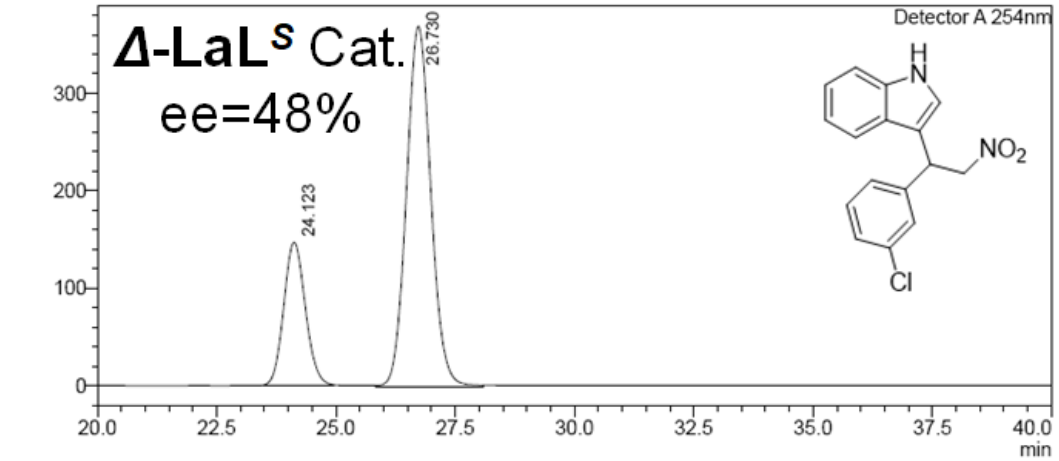

<Peak Table>

Detector A 254nm

Peak#	Ret. Time	Area	Height	Conc.	Unit	Mark	Name
1	24.123	4612041	146598	25.933		M	
2	26.730	13172239	369282	74.067		M	
Total		17784280	515880				

Fig. S56 HPLC spectrum of the Friedel-Crafts product 3-(1-(3-chlorophenyl)-2-nitroethyl)-1H-indole catalyzed by ***Δ*-LaL^S**.

<Chromatogram>

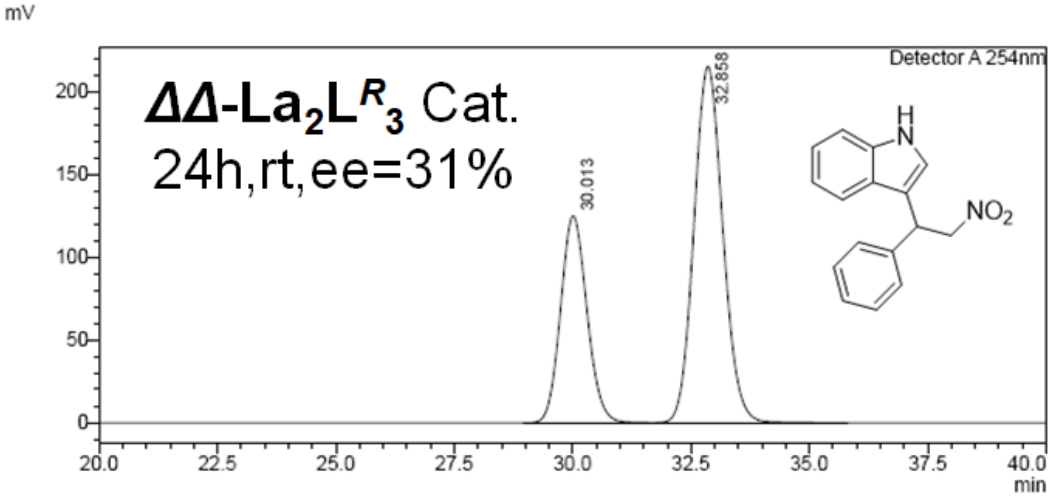

<Peak Table>

Detector A 254nm

Peak#	Ret. Time	Area	Height	Conc.	Unit	Mark	Name
1	30.013	4850869	124926	34.635			
2	32.858	9154788	215233	65.365		V	
Total		14005657	340158				

Fig. S57 HPLC spectrum of the Friedel-Crafts product 3-(2-nitro-1-phenylethyl)-1H-indole catalyzed by ***ΔΔ*-La$_2$L$^S_3$** (24h, rt).

<Chromatogram>

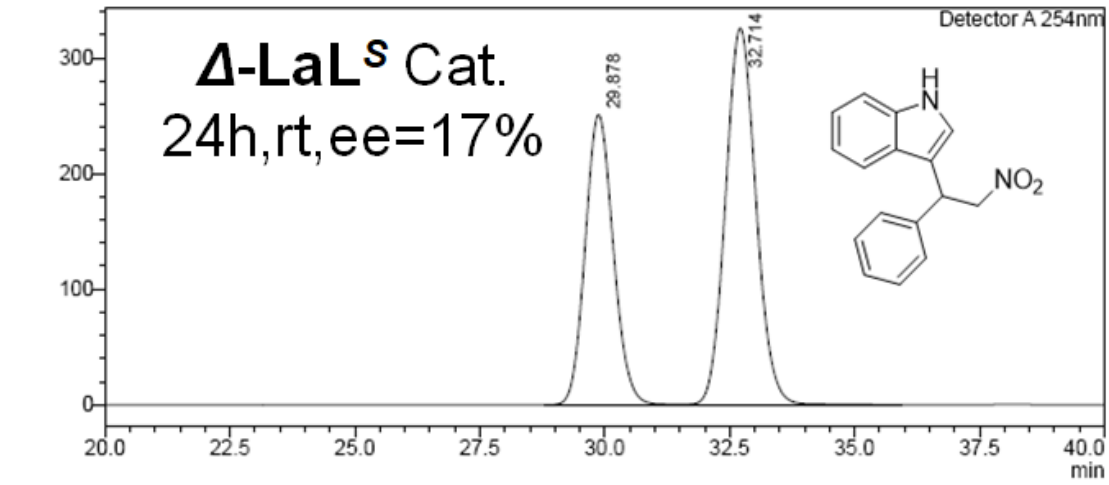

<Peak Table>

Detector A 254nm

Peak#	Ret. Time	Area	Height	Conc.	Unit	Mark	Name
1	29.878	9818587	250911	41.500			
2	32.714	13840611	325553	58.500		V	
Total		23659198	576464				

Fig. S58 HPLC spectrum of the Friedel-Crafts product 3-(2-nitro-1-phenylethyl)-1H-indole catalyzed by ***Δ*-LaL^S** (24h, rt).

7. X-ray single crystal diffraction analyses

Suitable single crystals for complexes ***ΛΛ*-La$_2$L$^{R}_{3}$**, ***Λ*-LaL^{R}** and ***Λ*-LaL^{R}G^{S}** were obtained by slow diffusion of poor solvent vapor DCM, CHCl3 and EA into the complexes solution of acetonitrile in after several days. Intensities for Eu4(**L1**)4 were carried out on Bruker D8 VENTURE photon II diffractometer with Iμs 3.0 microfocus X-ray source using APEX III program. Data reduction was performed with the saint and SADABS package. All the structures were solved by direct methods and refined by full matrix least-squares on *F2* with anisotropic displacement using the SHELXTL software package[2]. Because of the large amount of solvents that could not be fully located, the final R factors were slightly high. The electron residuals in such cases were removed by the SQUEEZE routine[3].

The steric maps and buried volumes[4] of these structures were calculated from https://www.molnac.unisa.it/OMtools/sambvca2.1/index.html.

Table S3. Crystal data and structure refinement for $\Lambda\Lambda$-$La_2L^R_3$.

Identification code	La2LR3	
Empirical formula	C196 H156 F18 La2 N38 O26 S6	
Formula weight	4271.78	
Temperature	130(2) K	
Wavelength	0.71073 Å	
Crystal system	Triclinic	
Space group	P1	
Unit cell dimensions	a = 18.2003(16) Å	□ = 66.480(2)°.
	b = 18.2134(16) Å	□ = 72.694(3)°.
	c = 18.9271(16) Å	□ = 88.242(3)°.
Volume	5464.6(8) $Å^3$	
Z	1	
Density (calculated)	1.298 Mg/m^3	
Absorption coefficient	0.528 mm^{-1}	
F(000)	2178	
Crystal size	0.20 x 0.10 x 0.10 mm^3	
Theta range for data collection	2.250 to 27.677°.	
Index ranges	-23<=h<=23, -23<=k<=23, -24<=l<=24	
Reflections collected	177998	
Independent reflections	50401 [R(int) = 0.0797]	
Completeness to theta = 25.242°	99.9 %	
Refinement method	Full-matrix least-squares on F^2	
Data / restraints / parameters	50401 / 2516 / 2551	
Goodness-of-fit on F^2	1.004	
Final R indices [I>2sigma(I)]	R1 = 0.0582, wR2 = 0.1410	
R indices (all data)	R1 = 0.0843, wR2 = 0.1561	
Absolute structure parameter	0.031(4)	
Extinction coefficient	n/a	
Largest diff. peak and hole	1.324 and -1.148 e.$Å^{-3}$	

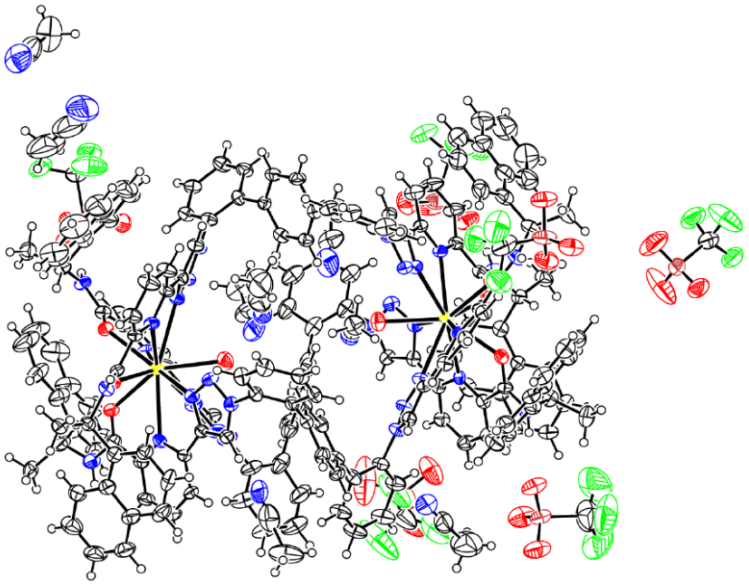

Fig. S59 Ortep drawing of the asymmetry unit in the crystal structure of $\Lambda\Lambda$-$La_2L^R_3$.

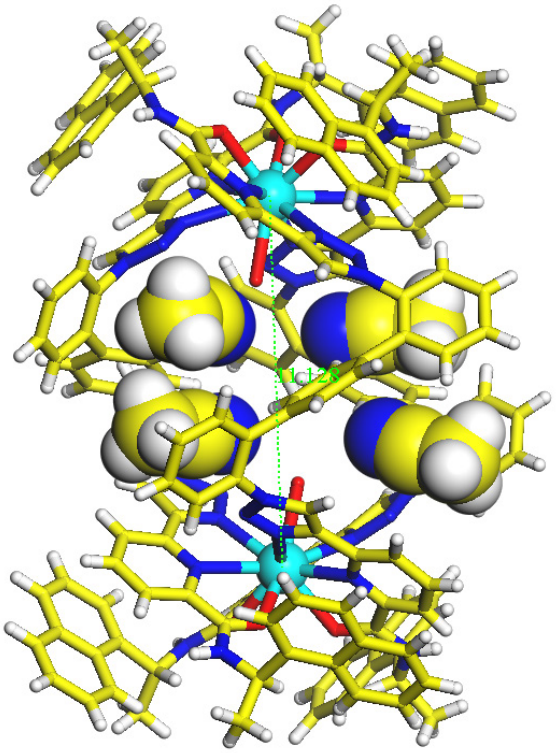

Fig. S60 The crystal structure of $\Lambda\Lambda$-$La_2L^R_3$ encapsulating four CH_3CN molecules.

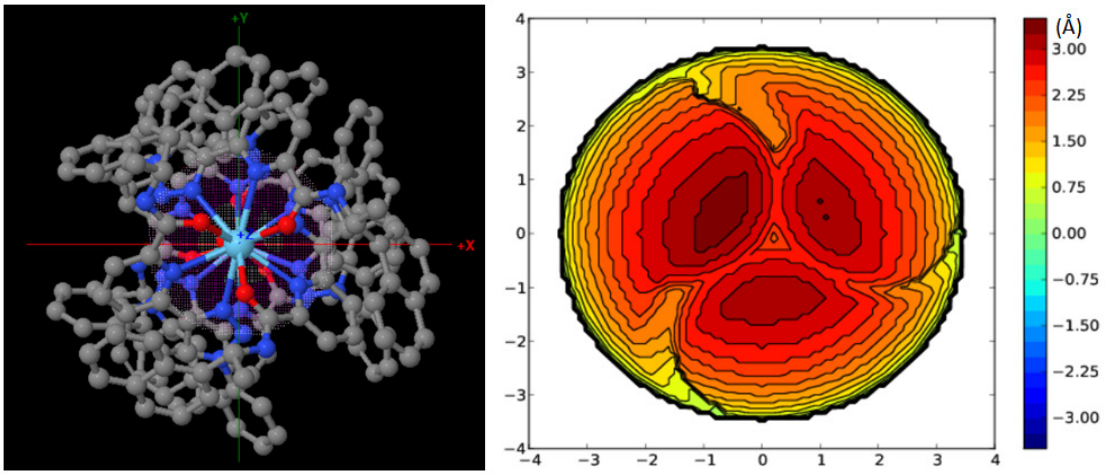

Fig. S61 Calculated orientation (left) and steric map (right) of La^{III} center in ***ΛΛ*-$La_2L^R_3$**.

Table S4. Buried volume ($\%V_{Bur}$) of La^{III} center in ***ΛΛ*-$La_2L^R_3$**.

Quadrant	SW	NW	NE	SE	Average
$\%V_{Bur}$	79.8	82.9	88.0	84.7	83.8

Table S5. Crystal data and structure refinement for ***Λ*-LaL^{R}**.

Identification code	LaLR
Empirical formula	C60 H44 La F6 N10 O10 S2 [+ solvent]
Formula weight	1382.09
Temperature	100(2) K
Wavelength	0.71073 Å
Crystal system	Orthorhombic
Space group	$P2_12_12_1$
Unit cell dimensions	a = 20.2522(8) Å □ = 90°.
	b = 22.2469(9) Å □ = 90°.
	c = 32.4795(13) Å □ = 90°.
Volume	14633.6(10) Å^3
Z	8
Density (calculated)	1.255 Mg/m^3
Absorption coefficient	0.711 mm^{-1}
F(000)	5576
Crystal size	0.1 x 0.07 x 0.07 mm^3
Theta range for data collection	1.109 to 23.275°.
Index ranges	-22<=h<=22, -24<=k<=24, -36<=l<=36
Reflections collected	83248
Independent reflections	21047 [R(int) = 0.0814]
Completeness to theta = 23.275°	99.9 %
Refinement method	Full-matrix least-squares on F^2
Data / restraints / parameters	21047 / 1709 / 1351
Goodness-of-fit on F^2	1.020
Final R indices [I>2sigma(I)]	R1 = 0.0802, wR2 = 0.2210
R indices (all data)	R1 = 0.1143, wR2 = 0.2503
Absolute structure parameter	0.043(9)
Extinction coefficient	n/a
Largest diff. peak and hole	1.479 and -1.869 e.Å^{-3}

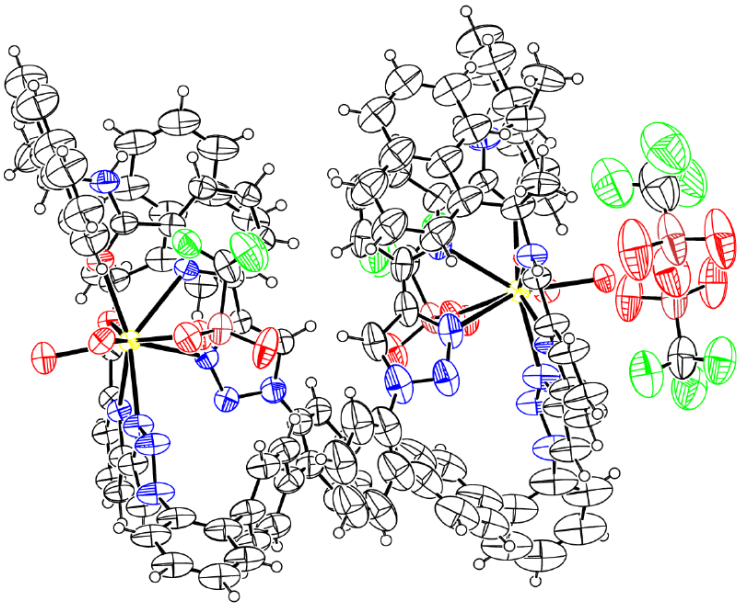

Fig. S62 Ortep drawing of the asymmetry unit in the crystal structure of ***Λ*-LaL^{R}**.

Table S6. Buried volume (%V_{Bur}) of La^{III} center in ***Λ*-LaL^{R}**.

Quadrant	SW	NW	NE	SE	Average
%V_{Bur}	79.6	52.6	25.8	82.3	60.1

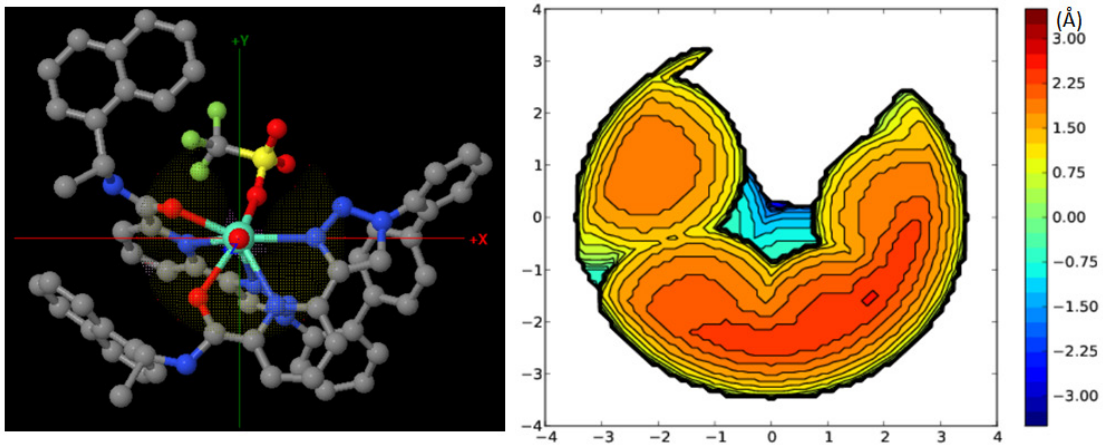

Fig. S63 Calculated orientation (left) and steric map (right) of La^{III} center in ***Λ*-LaL^{R}**.

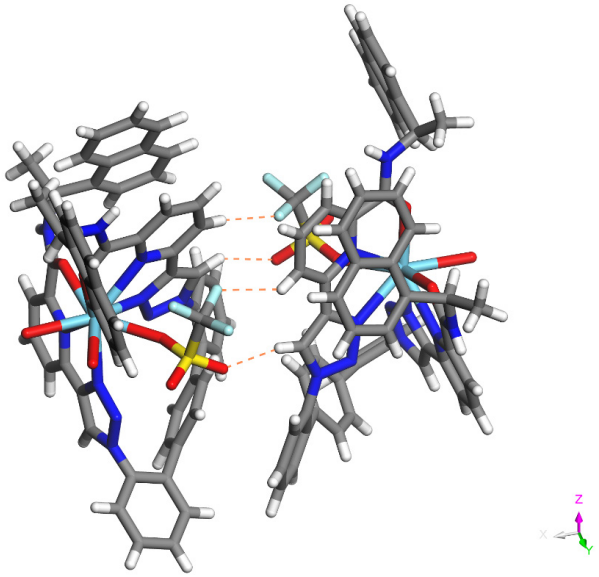

Fig. S64 Dimeric structure of ***Λ*-LaL^{R}** stabilized by hydrogen-bonding interactions.

Table S7. Crystal data and structure refinement for ***Λ*-LaL^{R}G^{S}**.

Identification code	LaLRGS	
Empirical formula	C84 H63 F9 La N13 O13 S3[+ solvent]	
Formula weight	1868.57	
Temperature	298(2) K	
Wavelength	0.71073 Å	
Crystal system	Orthorhombic	
Space group	$P2_12_12_1$	
Unit cell dimensions	a = 13.9577(6) Å	a= 90°.
	b = 18.1481(9) Å	b= 90°.
	c = 73.931(3) Å	g = 90°.
Volume	18727.2(14) Å^3	
Z	8	
Density (calculated)	1.326 Mg/m^3	
Absorption coefficient	0.604 mm^{-1}	
F(000)	7000	
Crystal size	0.1 x 0.08 x 0.08 mm^3	
Theta range for data collection	2.204 to 20.389°.	
Index ranges	-13<=h<=8, -17<=k<=16, -72<=l<=43	
Reflections collected	30260	
Independent reflections	18495 [R(int) = 0.0564]	
Completeness to theta = 20.389°	98.5 %	
Refinement method	Full-matrix least-squares on F^2	
Data / restraints / parameters	17816 / 2439 / 1615	
Goodness-of-fit on F^2	0.931	
Final R indices [I>2sigma(I)]	R1 = 0.0799, wR2 = 0.2180	
R indices (all data)	R1 = 0.1115, wR2 = 0.2574	
Absolute structure parameter	0.036(10)	
Extinction coefficient	n/a	
Largest diff. peak and hole	1.058 and -0.857 e.Å^{-3}	

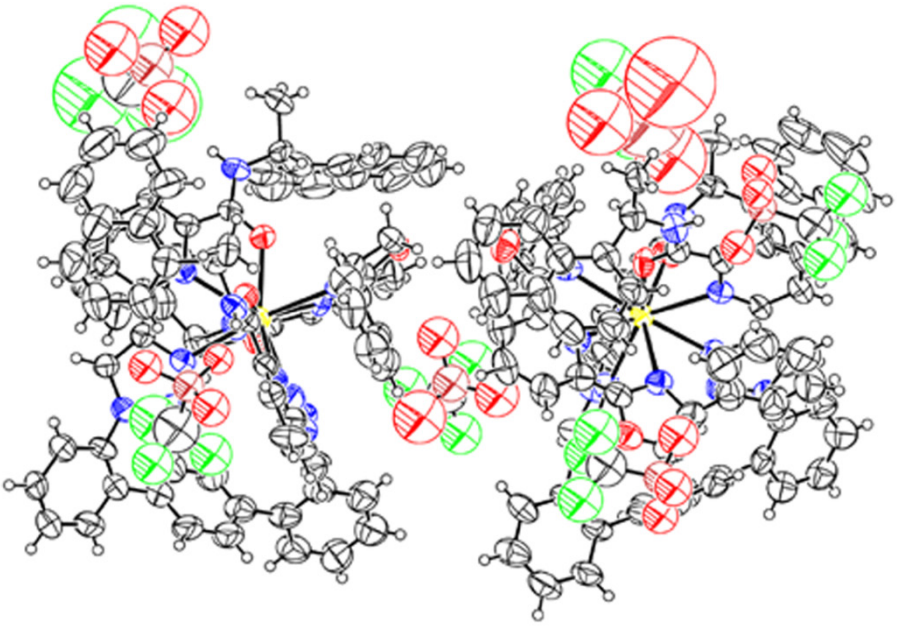

Fig. S65 Ortep drawing of the asymmetry unit in the crystal structure of ***Λ*-LaL^{R}G^{S}**.

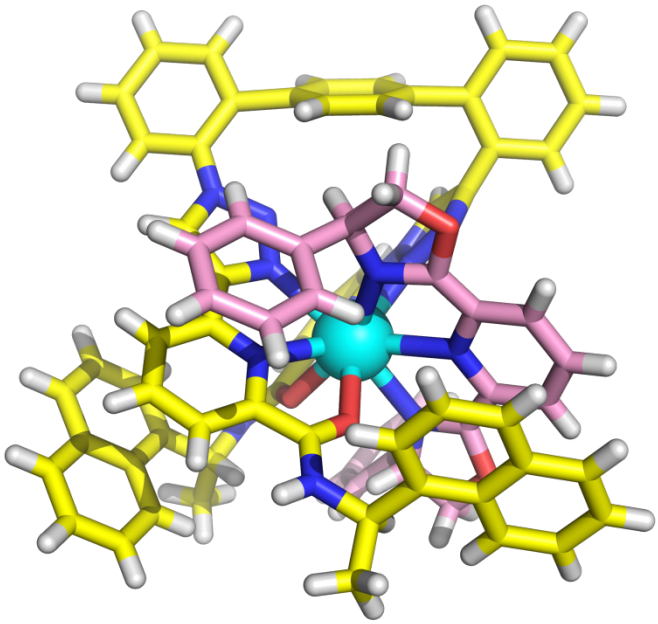

Fig. S66 X-ray single crystal structure of ***Λ*-LaL^{R}G^{S}**. La: cyan, C: yellow (pink for **G^{S}**), H: white, N: blue, O: red. Anions located outside are omitted for clarity.

Table S8. Buried volume (%V_{Bur}) of La^{III} center in ***Λ*-LaL^{R}G^{S}**.

Quadrant	SW	NW	NE	SE	Average
%V_{Bur}	88.8	88.6	93.2	93.0	90.9

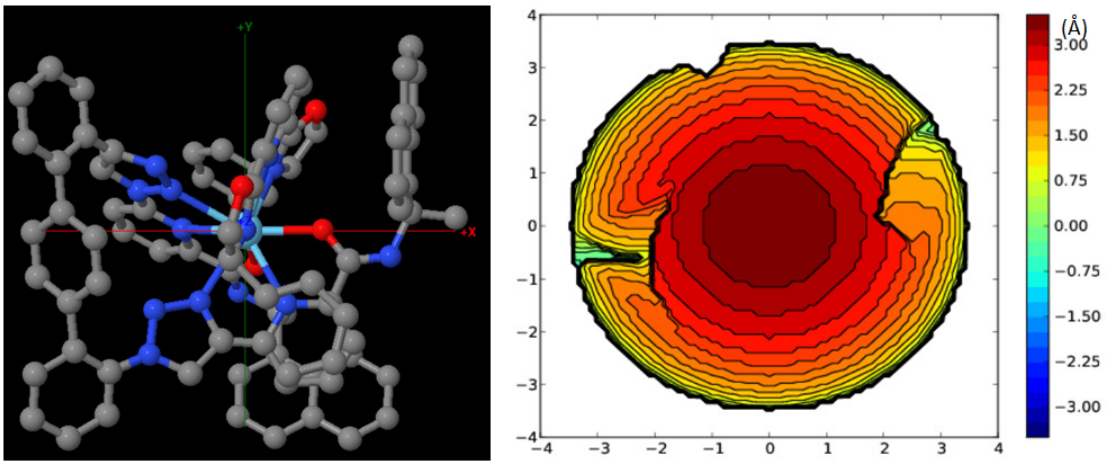

Fig. S67 Calculated orientation (left) and steric map (right) of La^{III} center in ***Λ*-LaL^{R}G^{S}**.

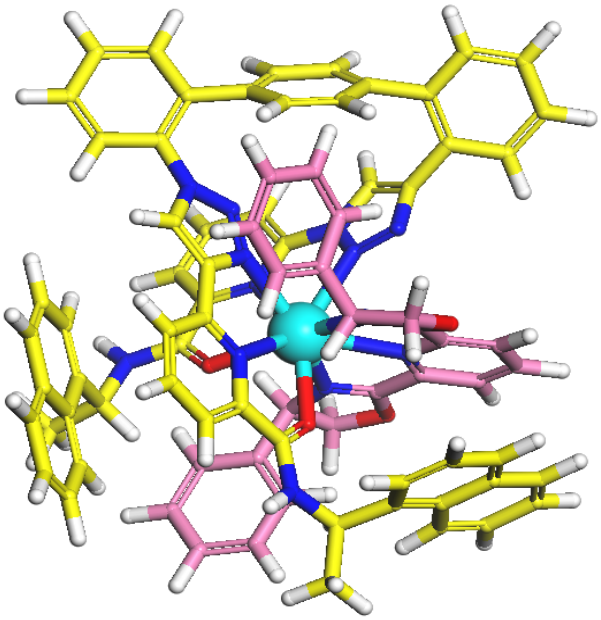

Fig. S68 Calculated structure of ***Λ*-LaL^{R}G^{R}**. La: cyan, C: yellow (pink for **G^{S}**), H: white, N: blue, O: red.

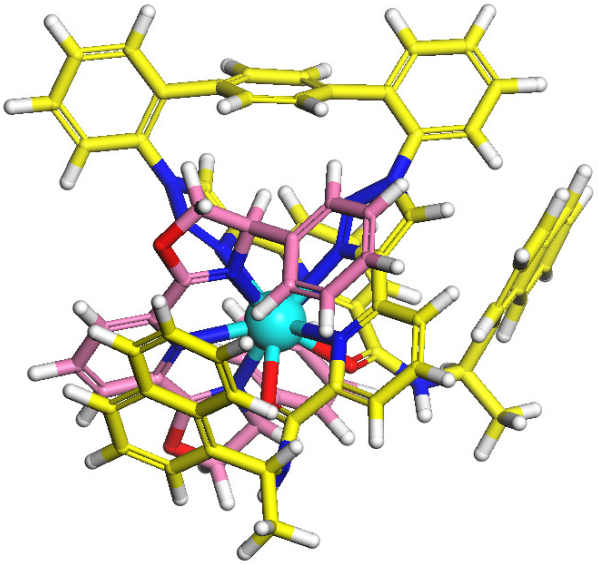

Fig. S69 Calculated structure of ***Δ*-LaL^{R}G^{R}**. La: cyan, C: yellow (pink for **G^{S}**), H: white, N: blue, O: red.

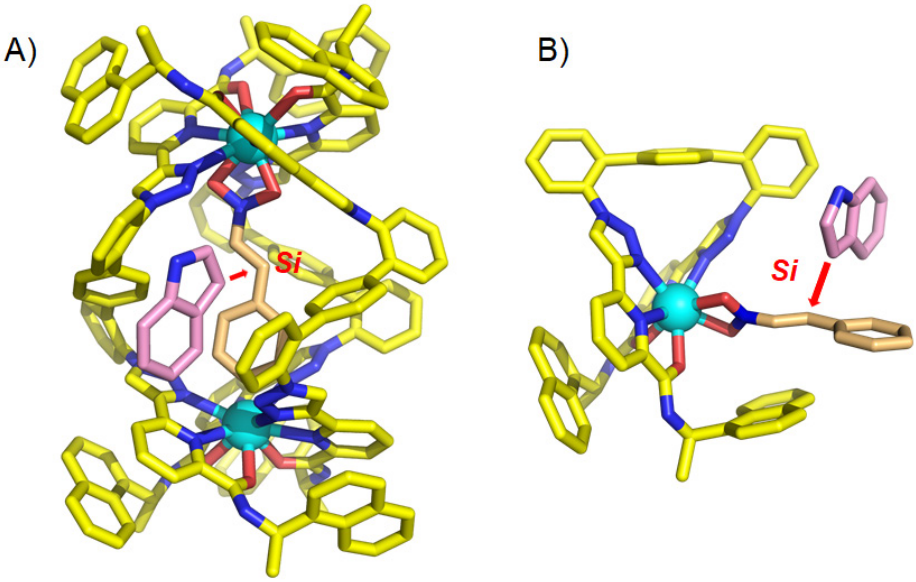

Fig. S70 Proposed transition state models for the Friedel-Crafts alkylation reaction of indole and trans-β-nitrostyrene catalysed by A) ***ΛΛ*-La$_2$L$^{R}_3$** and B) ***Λ*-LaL^{R}**. La: cyan, C: yellow (pink for indole and light orange for trans-β-nitrostyrene), N: blue, O: red, H atoms were omitted for clarity.

8. Supporting references

1. X. Q. Guo, L. P. Zhou, L. X. Cai and Q. F. Sun, Self-assembled bright luminescent lanthanide-organic polyhedra for ratiometric temperature sensing, *Chem. Eur. J.*, 2018, **24**, 6936-6940.
2. G. M. Sheldrick, A short history of SHELX, *Acta Crystallogr. Sect. A*, 2008, **64**, 112-122.
3. (a)A. L. Spek, Single-crystal structure validation with the program PLATON, *J. Appl. Crystallogr.*, 2003, **36**, 7-13; (b)A. L. Spek, PLATON SQUEEZE: a tool for the calculation of the disordered solvent contribution to the calculated structure factors, *Acta Crystallogr. Sect. C-Struct. Chem.*, 2015, **71**, 9-18.
4. L. Falivene, Z. Cao, A. Petta, L. Serra, A. Poater, R. Oliva, V. Scarano and L. Cavallo, Towards the online computer-aided design of catalytic pockets, *Nat. Chem.*, 2019, **11**, 872-879.